Am J Cancer Res 2026;16(4):1509-1539
www.ajcr.us /ISSN:2156-6976/ajcr0173052

Original Article

From locus to gene: causal inference and experimental validation prioritize PSMA4 as a candidate target in lung adenocarcinoma

Hui Lu*, Sai Wang*, Yuhang Ma, Zhiming Shen, Long Yao, Ningning Kang, Panpan Si, Renquan Zhang

Department of Thoracic Surgery, The First Affiliated Hospital of Anhui Medical University, Hefei, Anhui, China.
**Equal contributors.*

Received April 2, 2026; Accepted April 21, 2026; Epub April 25, 2026; Published April 30, 2026

Abstract: Lung adenocarcinoma (LUAD) remains a leading cause of cancer-related mortality worldwide, and although targeted therapy and immunotherapy have improved clinical outcomes, their long-term efficacy is frequently limited by therapeutic resistance, underscoring the need to identify additional biologically relevant and potentially actionable targets. In this study, we applied summary-data-based Mendelian randomization (SMR) by integrating lung cancer genome-wide association study (GWAS) summary statistics with cis-expression quantitative trait locus (cis-eQTL) and cis-methylation quantitative trait locus (cis-mQTL) datasets to prioritize candidate genes associated with LUAD risk. The robustness of SMR-significant signals was further evaluated using the heterogeneity in dependent instruments (HEIDI) test and Bayesian colocalization analysis. Independent transcriptomic datasets from the Gene Expression Omnibus (GEO), together with multiple public databases, were used for expression and prognostic validation, while protein-protein interaction (PPI) and functional enrichment analyses were performed to provide mechanistic context. Among 13 genes prioritized by integrative genetic analyses, PSMA4 (Proteasome 20S Subunit Alpha 4) emerged as the leading LUAD-relevant candidate on the basis of convergent multi-omics evidence, colocalization support, reproducible overexpression (OE) across independent cohorts, and adverse prognostic association. Functional experiments demonstrated that PSMA4 knockdown (KD) suppressed LUAD cell proliferation, migration, invasion, and xenograft tumor growth, whereas PSMA4 overexpression produced the opposite effects. Mechanistically, PSMA4 interacted with p53 and facilitated the proteasome-dependent turnover of ubiquitinated p53, as supported by co-immunoprecipitation, immunofluorescence, ubiquitination, proteasome inhibition, and cycloheximide chase assays, thereby attenuating p53 signaling. Collectively, these findings support PSMA4 as a biologically relevant and potentially actionable target in LUAD and provide a mechanistic rationale for further translational investigation.

Keywords: Lung adenocarcinoma, summary-data-based Mendelian randomization, HEIDI test, PSMA4, multi-omics analysis, proteasome, therapeutic target

Introduction

Lung cancer is a common lethal malignant tumor in China, adding a burden to medicine and society. In 2022, data from the National Cancer Center showed that there were 1,060,600 new cases of lung cancer and 733,300 death cases, with both the incidence rate and mortality rate ranking first [1]. Aging, smoking, second-hand smoke, cooking fumes, and air pollution have increased the burden of lung cancer [2]. More than 80% of lung cancer cases are non-small cell lung cancer (NSCLC), and about 75% are diagnosed at an advanced stage [3]. The 5-year survival rate of lung cancer patients is about 15%, and the prognosis is poor [4]. Lung adenocarcinoma (LUAD) belongs to the main subtype of non-small cell lung cancer (NSCLC), with a high incidence and mortality rate [3, 5]. Recently, the treatment model of lung adenocarcinoma has been improved, and there have been key breakthroughs in targeted and immunotherapy [6].

For lung adenocarcinoma patients with driver gene mutations, targeted therapy is the key.

https://doi.org/10.62347/XJJZ8847

The population with specific genomic abnormalities gets obvious clinical benefits from molecular targeted drugs [7], and nearly 69% of advanced NSCLC patients have clinically actionable targets [8]. Approved targeted drugs cover the situations of gene mutations such as EGFR, ALK, ROS1, BRAF, etc. As a first-line treatment, EGFR-TKIs such as osimertinib can prolong the median progression-free survival (PFS) to 18.9 months, which is better than chemotherapy [7, 9].

Immunotherapy is a key means of cancer treatment. PD-1/PD-L1 inhibitors are beneficial for patients with advanced cancer [10]. In the KEYNOTE-024 trial, Reck et al. the report says that the 6-month survival of high PD-L1 patients treated with pembrolizumab is higher than the overall survival (OS) of the chemotherapy group [11].

There is progress in this regard, but the efficacy of targeted and immune therapies is still not very good. The challenge for key efficacy improvement is due to the immunosuppression of the tumor microenvironment (infiltration of regulatory T cells, expansion of myeloid-derived suppressor cells), and problems in antigen presentation (for example. The situation of HLA loss occurs, and the interferon-γ signaling pathway is dysregulated [12]). Recently, some studies have explored combination immunotherapy such as PD-1 and CTLA-4 inhibitors, or chemotherapy regimens, but some patients still have disease progression due to the occurrence of drug resistance [13]. Immunotherapy failure lacks standardized rescue regimens, so there is an urgent need for predictive biomarkers (such as tumor mutation burden TMB, STK11 mutation) to guide precision therapy [14]. New therapeutic targets need to be sought to overcome limitations, thereby proposing new lung cancer therapies.

Summary-data-based Mendelian randomization (SMR) is a method to improve Mendelian randomization (MR) causal inference by integrating genome-wide association study (GWAS) and quantitative trait locus (QTL) data. This method strictly analyzes genetic associations and also enhances statistical power. Using genetic variations (mainly single nucleotide polymorphisms (SNPs)) as instrumental variables (IVs), regression techniques are employed to evaluate the causal relationship between exposure factors (such as gene expression or DNA methylation [DNAm]) and disease outcomes [15, 16]. A key advantage of SMR is to reduce confounding factors in observational studies, reverse causal bias, and greatly improve the reliability of causal inference [17]. The framework assumes that the IV only affects outcomes through specific exposures. The HEIDI (Heterogeneity in Dependent Instruments) test is used to remove SNPs with pleiotropy to ensure the specificity of detecting associations [18]. SMR is often used in the study of complex diseases, such as cardiovascular diseases, cancers, immune diseases, etc. For example, Zhu et al. used SMR to show the causal effect of FTO gene expression on obesity risk [19], and Yang et al. analyses combining single-sample Mendelian randomization (SMR) with single-cell RNA sequencing (RNA-seq) revealed that the expression of LGALS9, which is associated with the onset of sepsis, was decreased [20]. SMR has been confirmed to have certain roles in drug target discovery. Integrating genome-wide association studies (GWAS) of plasma proteomes and disease outcome data can rapidly determine the causal association between the PCSK9 gene and low-density lipoprotein cholesterol (LDL-C), providing genetic verification for the development of PCSK9 inhibitors such as alirocumab [21]. Recently, Lin et al. used SMR to integrate data of expression quantitative trait loci (eQTL) and methylation quantitative trait loci (mQTL) to identify RELT, TNFSF12, ICAM5, and ERAP2 as new therapeutic targets for intracranial aneurysms [22].

In this context, this study first combines SMR with batch RNA-seq data to explore the roles of gene expression and DNAm in the pathogenesis of lung cancer. The analytical framework includes multi-omics verification, colocalization analysis, and Gene Expression Omnibus (GEO) datasets confirmation. In vitro and in vivo experiments are also carried out for functional verification. This multi-level strategy aims to find new therapeutic targets and construct a genetic evidence chain for the pathogenesis of lung cancer.

Materials and methods

This study adopted a multi-omics integrative analysis strategy (**Figure 1**). First, we systematically compiled the aggregated data from

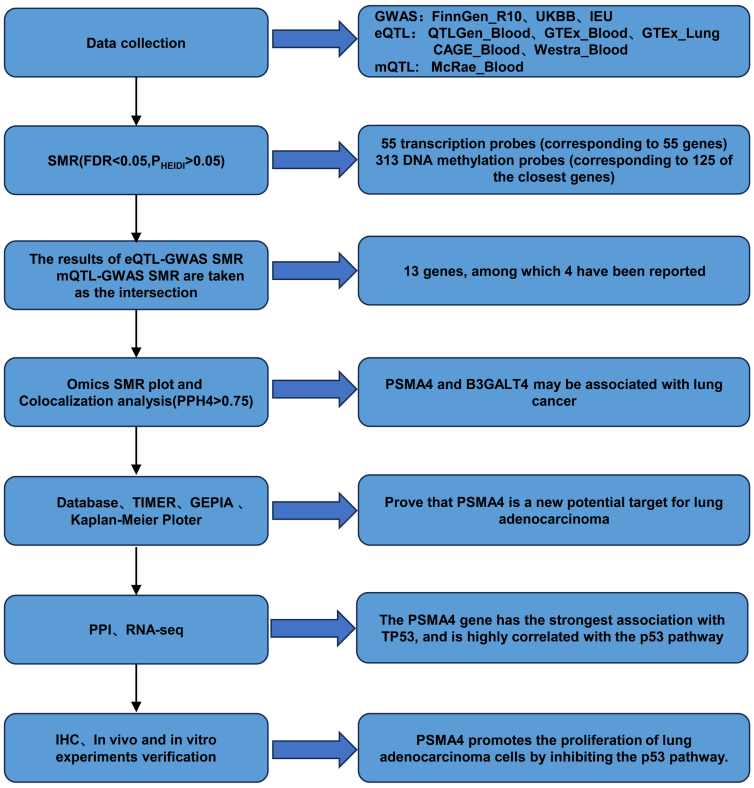

Figure 1. Summary of study design, methods of analysis, and critical process. Abbreviations: SMR, summary data-based Mendelian randomization; GWAS, the genome-wide association study; eQTL, expression quantitative trait loci; mQTL, methylation Quantitative Trait Loci; HEIDI test, heterogeneity in dependent instruments test; PP.H4, the posterior probability of hypothesis 4; GEO, the Gene Expression Omnibus; TCGA_GTEx, The Cancer Genome Atlas database combined with Genotype-Tissue Expression database; PPI, Protein-Protein Interaction Network; IHC, immunohistochemistry; PSMA4, Proteasome 20S Subunit Alpha 4.

GWAS, eQTL, and mQTL datasets from various sources. Next, we performed SMR association analyses for eQTL-GWAS and mQTL-GWAS. Subsequently, the HEIDI test was applied to remove pleiotropic interference. Finally, colocalization analysis was conducted on the significant loci to screen for candidate genes exhibiting a potential causal relationship with lung cancer.

To validate the screening results, we leveraged bulk RNA-seq transcriptome data and other authoritative online databases for cross-validation. We constructed protein-protein interaction (PPI) networks for the key candidate genes and performed Gene Ontology (GO)/Kyoto Encyclopedia of Genes and Genomes (KEGG) pathway enrichment analyses to elucidate their molecular mechanisms. The final candidate genes were then validated by immunohistochemical (IHC) analysis of clinical specimens, *in vitro* phenotypic assays, and *in vivo* nude mouse tumor formation experiments.

SMR analysis

Research design and data sources: To investigate the potential causal links between candidate genes and lung cancer susceptibility, we adopted the SMR method for systematically combining eQTL, mQTL, and pooled GWAS data in relation to LUAD.

Genetic association data for lung cancer were sourced from several authoritative GWAS databases, including FinnGen (version R10), UK Biobank, and IEU OpenGWAS (**Table 1**). Gene expression quantitative trait data were obtained from the following eQTL resources: eQTLGen (n = 31,684), Genotype-Tissue Expression (GTEx, version R8; n_blood = 670, n_lung = 515), Cap Analysis of Gene Expression (n = 2765), and Westra (n = 3511) (**Table 2**). In addition to peripheral blood transcriptome measurements, this study incorporated lung tissue-specific expression data from the GTEx database. DNAm data originated from a large-scale blood mQTL meta-analysis conducted by McRae et al. (sample size n = 614) (**Table 2**). All summary-level datasets were derived from European ancestry populations.

To ensure analytical rigor, the following quality control standards were implemented: (1) for eQTL and mQTL data, SMR analysis incorporated only probes with at least one cis-QTL exceeding the genome-wide significance threshold ($P < 5 \times 10^{-8}$); (2) the cis-regulatory region was defined as the genomic interval extending 2 Mb upstream and downstream of each probe; and (3) all datasets were harmonized to genome build hg38 by using the

Table 1. Summary of GWAS data information

Data sources	Filename	Year	Tissue	Ancestry	Number of SNPs	Build
FinnGen_R10	C3_NSCLC_ADENO_EXALLC	2023	Blood	European	19,814,823	hg38
	C3_NSCLC_SQUAM_EXALLC	2023	Blood	European	19,814,815	hg38
	C3_BRONCHUS_LUNG_EXALLC	2023	Blood	European	19,814,950	hg38
	C3_LUNG_NONSMALL_EXALLC	2023	Blood	European	19,814,916	hg38
UKBB	LUNG_CANCER	2018	Blood	European	10,455,414	hg19
IEU	ukb-b-20176 illnesses of mother: Lung cancer	2018	Blood	European	9,851,867	hg19
	ukb-b-14521 illnesses of father: Lung cancer	2018	Blood	European	9,851,867	hg19
	ieu_b_4955	2021	Blood	European	11,078,115	hg19

Note: Abbreviations: GWAS, genome-wide association studies; SNPs, single nucleotide polymorphisms.

Table 2. Source and detailed information of QTL data

Data category	Data sources	Ancestry	Tissue	Number of SNPs	Build
Cis-eQTL	QTLGen	European	Blood	10,078,879	hg19
	GTEx	European	Blood	1,609,254	hg19
	GTEx	European	Lung	1,565,899	hg19
	CAGE	European	Blood	6,322,664	hg19
	Westra	European	Blood	519,879	hg19
Cis-mQTL	McRae	European	Blood	30,985,683	hg19

Note: Abbreviations: QTL, quantitative trait loci; Cis-eQTL, cis-expression quantitative trait locus; Cis-mQTL, cis-methylation quantitative trait locus; SNPs, single nucleotide polymorphisms.

"hg19ToHg38.over.chain.gz" R package to maintain genomic coordinate consistency.

SMR and HEIDI test for detecting pleiotropic associations: The SMR method uses a single genetic variant - usually an SNP - as an IV to evaluate the relationship between an exposure and an outcome. The two-sample MR analysis assumes that Z is the tool variable (genetic variation), X is the exposure, and Y is the outcome. b_{zx} represents the influence of the tool variable on the exposure, b_{zy} represents the influence of the tool variable on the outcome, and b_{xy} represents the influence of the exposure on the outcome. According to the two-stage least squares method, b_{XY} is calculated as follows:

$$b_{XY} = \frac{b_{ZY}}{b_{ZX}} \quad \text{(Formula 2-1)}$$

In the SMR method, the SNP effect of the QTL data on X, denoted as β_{ZX}, is regarded as an unbiased estimate of b_{ZX}. Subsequently, b_{XY} is determined as follows:

$$b_{XY} = \frac{b_{ZY}}{\beta_{ZX}} \quad \text{(Formula 2-2)}$$

By using the delta method [23, 24], the variance of b_{XY} is estimated using the following formula:

$$var(b_{XY}) \approx \frac{b_{ZY}^2}{\beta_{ZX}^2}\left[\frac{var(\beta_{ZX})}{b_{ZX}^2} + \frac{var(b_{ZY})}{b_{ZY}^2} - \frac{2cov(b_{ZX}, b_{ZY})}{\beta_{ZX} b_{ZY}}\right] \quad \text{(Formula 2-3)}$$

The significance of b_{XY} was tested using the statistic T_{SMR}, which was estimated as follows [23]:

$$T_{SMR} = \frac{b_{XY}^2}{var(b_{XY})} \quad \text{(Formula 2-4)}$$

We utilized lung cancer as the outcome variable, QTLs as the exposure variable, and SNPs as the IV in a causal inference analysis. Notably, because SMR analysis based on a single genetic variation cannot effectively differentiate between authentic causal relationships and pleiotropic effects, the identified association results in this study should be regarded as inferential evidence of causal relationships.

To strengthen causal inference, we conducted the HEIDI test to assess IV validity under the null hypothesis of a single causal variant. Strict quality control measures were implemented as follows: 1. A 2 Mb window was defined around

each probe. 2. eQTLs/mQTLs significant at $P < 5.0 \times 10^{-8}$ were selected for SMR analysis. 3. In the HEIDI test, a *P*-value threshold of 1.57×10^{-3} (equivalent to $\chi^2 = 10$) was considered for QTL. 4. SNPs in high linkage disequilibrium (LD) ($r^2 > 0.90$ or $r^2 < 0.05$) with the lead QTL were excluded.

We confined our analyses of DNAm and gene expression to cis-regulatory regions (< 2 Mb). The Benjamini - Hochberg method was used to control the false discovery rate (FDR) in all SMR tests by employing the 1000 Genomes Project European data as the LD reference.

Trajectory visualization analysis: On the basis of the SMR results, we applied stringent statistical criteria (FDR < 0.05 and p_HEIDI > 0.05) for gene selection. Genes exhibiting significant associations in both eQTL-GWAS and mQTL-GWAS SMR analyses were prioritized for further validation. Visual confirmation was subsequently performed using the SMR online analysis platform (SMR Portal, https://yanglab.westlake.edu.cn/smr-portal). We uploaded curated lung cancer GWAS summary statistics to the platform and selected the corresponding eQTL datasets (eQTL_eQTLGen, eQTL_GTEx_Whole_Blood, and eQTL_GTEx_Lung) along with mQTL data (mQTL_McRae). The parameters p_SMR and p_HEIDI were set to 1e-05 and 5e-02, respectively. The genes with significant correlations obtained from the platform analysis were systematically recorded and organized for subsequent in-depth analysis.

Colocalization analysis: To elucidate potential causal relationships between genes and lung cancer while accounting for confounding factors by LD, we performed Bayesian colocalization analysis using the "coloc" R package. This approach evaluates five competing hypotheses: H0 (null hypothesis): there is no causal variation between the gene and lung cancer; H1: there is only a single causal variation in the gene; H2: there is only a single causal variation in lung cancer; H3: there are two independent causal variations between the gene and lung cancer; and H4: SNPs within the co-location region and the two traits have a significant correlation and are driven by the same causal locus. The posterior probability for H4 (PP.H4) serves as the primary metric for colocalization evidence, where higher values indicate greater confidence that gene expression and lung cancer risk share standard causal mechanisms. We considered results with PP.H4 ≥ 0.75 as strong evidence for colocalization according to the established standards in the field.

Assumptions and limitations of SMR/colocalization analyses: This study uses SMR analysis with cis-QTLs as instrumental variables to infer latent associations between exposures (e.g. gene expression or DNA methylation) and outcomes (e.g. disease risk), based on aggregated statistical data. The validity of this method depends on two key assumptions. First, the selected genetic instrumental variables must be strongly correlated with the exposure factors. Second, the instrumental variable must primarily influence disease risk through the exposure factor rather than through other pathways, such as pleiotropy. It should be noted that, due to LD, correlated genetic variants may represent different causal signals. Consequently, observed SMR associations may originate from shared causal variation, or they may merely reflect two adjacent yet independent causal variants within the LD interval. To mitigate the risk of misinterpretation, we employed the HEIDI heterogeneity test to filter out inconsistent signals and conducted a Bayesian co-localisation analysis to determine whether GWAS and QTL signals might be driven by the same causal variant.

Nevertheless, we are aware that neither the HEIDI test nor co-localisation analysis can rule out the influence of pleiotropy or LD-related confounding factors entirely. The efficacy of both methods is constrained by factors including sample size, the selected LD reference panel and model prior settings. Therefore, when interpreting our findings, we treat the genetic evidence provided by SMR as a basis for prioritising candidate genes rather than drawing definitive causal conclusions. This genetic prioritisation was ultimately supported and supplemented by subsequent independent transcriptomic validation and systematic functional experiments.

Bulk RNA-seq analysis and online database validation

To systematically validate the SMR-derived candidates, we implemented a multiplatform verification approach. First, transcriptomic datasets related to lung cancer were obtained

from the GEO database. The "GEOquery" package in R Studio (v4.2.3) was then used to perform differential expression analysis to assess variation in the expression of SMR-identified genes. Second, we utilized the online platforms GEPIA (Gene Expression Profiling Interactive Analysis) and TIMER (Cistrome Data Portal) to validate differences in gene expression between tumor and normal tissues, identify subtype differences, and conduct survival analyses. Finally, the online Kaplan-Meier Plotter database (kmplot.com) was used to input the desired genes, OS analysis was conducted according to the lung cancer stage, and differentially expressed genes with a significant prognostic value were identified.

PPI

As the main executors of cellular functions, the protein interaction networks play a central role in life processes. Proteins form complex regulatory networks through specific interactions, and deciphering these interaction-based relationships is crucial for understanding protein functions [25]. We utilized the STRING database (https://cn.string-db.org/) to analyze the interaction network of the candidate target proteins and used Cytoscape software version 3.10.3 to visualize the links between them.

Experimental verification

Collection of clinical specimens: Ten pathological specimens of LUAD and their corresponding adjacent normal lung tissues were collected from the First Affiliated Hospital of Anhui Medical University in 2025. The study was approved by the hospital's ethics committee (Approval No.: PJ2025-07-41), and informed consent was obtained from patients and their families. The specimens were formalin-fixed and paraffin-embedded for subsequent IHC analysis.

Cell culture and establishment of knockdown and overexpression systems: The following human lung cancer cell lines were obtained from the American Type Culture Collection (ATCC, Manassas, VA, USA): A549, PC-9, NCI-H1299, NCI-H838, SPC-A1, and SK-LU-1. The nonmalignant lung cancer cell line BEAS-2B was also obtained from the ATCC. All cell lines were cultured in Dulbecco' modified Eagle's medium supplemented with 10% fetal bovine serum (FBS, Gibco), 100 μg/mL chloramphenicol, and 100 U/mL penicillin (Shanghai Betain Biotechnology Co., Ltd.) at 37°C in a 5% CO_2 environment. All cell lines used in this study were obtained from ATCC and authenticated by short tandem repeat (STR) profiling. The identity of the cell lines was confirmed by comparing their STR profiles with the reference profiles maintained by ATCC. Mycoplasma detection was carried out using a PCR-based assay, and the results confirmed that the cell lines were mycoplasma-negative prior to experimentation.

To develop PSMA4 knockdown and overexpression cell systems, specific shRNA lentiviral vectors targeting PSMA4 and scramble shRNA negative control vectors (Qingke Biotechnology Company) without homologous sequences, PSMA4 overexpression lentiviral vectors, and empty vector controls (Qingke Biotechnology Company) were transfected into logarithmic growth phase cells. After 72 h of transfection, puromycin was added to screen for stably transfected cell lines.

Western blotting (WB) assay: Cellular proteins were solubilized in RIPA buffer (Beyotime, China), and their concentrations were determined using a bicinchoninic acid protein quantification kit (Beyotime). An equal amount of protein (30 μg per lane) was then electrophoretically resolved on sodium dodecyl sulfate-polyacrylamide gels and transferred onto polyvinylidene fluoride membranes through electroblotting. The membranes were blocked with 5% nonfat milk and incubated overnight at 4°C with primary antibodies against PSMA4 (Proteintech, Cat# 11943-2-AP, 1:2000), p53 (Proteintech, Cat# 10442-1-AP, 1:10000), p21 (Proteintech, Cat# 82669-2-RR, 1:1000), α-tubulin (Proteintech, Cat# 11224-1-AP, 1:10000), or vinculin (Proteintech, Cat# 26520-1-AP, 1:10000), followed by incubation for 1 h at room temperature with Multi-rAb® HRP-Goat Anti-Rabbit Recombinant Secondary Antibody (H+L) (Proteintech, Cat# RGAR001, 1:2000) or Multi-rAb® HRP-Goat Anti-Mouse Recombinant Secondary Antibody (H+L) (Proteintech, Cat# RGAM001, 1:2000), as appropriate. Protein bands were visualized using Western Bright ECL reagent (Advansta, USA), and band intensity was quantified using ImageJ software.

RNA extraction and quantitative real-time PCR (qPCR): Total RNA was extracted from transgenic A549 and PC-9 LUAD cells (including KD and OE variants) according to the manufacturer's instructions. RNA concentration and purity were measured using a NanoDrop spectrophotometer, and RNA samples were diluted to 200 ng/μL for reverse transcription. cDNA was synthesized using SweScript All-in-One RT SuperMix for qPCR (One-Step gDNA Remover) in a 20 μL reaction system containing 4 μL 5× SweScript All-in-One SuperMix, 1 μL gDNA Remover, 10 μL total RNA, and RNase-free water to a final volume of 20 μL. The reverse transcription program was as follows: 25°C for 5 min, 42°C for 30 min, and 85°C for 5 s.

qPCR was performed using 2× Universal Blue SYBR Green qPCR Master Mix on a real-time PCR system. Each 15 μL reaction contained 7.5 μL 2× Universal Blue SYBR Green qPCR Master Mix, 1.5 μL gene-specific primers, 2.0 μL cDNA template, and 4.0 μL nuclease-free water. The amplification conditions were as follows: initial denaturation at 95°C for 30 s, followed by 40 cycles of 95°C for 15 s and 60°C for 30 s. A melting curve analysis was performed from 65°C to 95°C, with fluorescence signal acquisition at each 0.5°C increment. Each sample was analyzed in triplicate. Gene expression levels were normalized to α-tubulin (TUBA1B) and calculated using the $2^{-\Delta\Delta CT}$ method. The primer sequences were as follows: PSMA4 forward: GATAAGCACTATGGCTTTCAGC; PSMA4 reverse: CTGCAGCGCTATTATTTCCAAT; TUBA1B forward: GTGCGTTACTTACCTCGACTCTT; TUBA1B reverse: AGCAGTAGTGGCTAGGGATTAG.

Cell function experiments: Cell Counting Kit-8(CCK-8) proliferation assay: A total of 3000 cells per well were seeded into a 96-well plate. After 0, 24, 48, and 96 h of culture, 10 μL of CCK-8 assay reagent was added to each well, and the samples were incubated for an additional 2 h. The absorbance value was measured at 450 nm by using a microplate reader.

Proliferation detection with 5-Ethynyl-2'-deoxyuridine (EdU) assay: Cell proliferation was assessed using the EdU detection kit (Abbkine). Cells were cultured in 96-well plates and incubated with 10 mM EdU (diluted 1:1000) for 2 h. After cell fixation, the Click-iT reaction mixture was prepared and applied (100 μL/well), followed by 30 min of incubation in the dark. The nuclei were stained with Hoechst 33342 (1×), and EdU-positive cells were visualized using a fluorescence microscope. The percentage of EdU-positive cells was then calculated.

Scratch healing experiments: Cells were cultured in 6-well plates until they reached confluence of over 90%. A straight scratch in the cell layer was then created using a sterile 200-μL pipette tip. Images of scratch wound healing were captured under a microscope at 0, 24, and 48 h after scratch creation, and changes in the wound area were quantified.

Clonogenic assay: A total of 500 cells were plated in a 6-well plate and cultivated for 2 weeks. Subsequently, the cells were fixed with 4% paraformaldehyde and stained with 0.1% crystal violet. The number of visible cell clusters containing more than 50 cells was then counted.

Transwell invasion assay: A Matrigel layer was placed in the upper chamber of the Transwell cell culture system. Next, cell suspension was added to the upper chamber containing a serum-free medium, and the lower chamber was filled with a medium containing 20% FBS. Following a 24-h incubation period, the noninvasive cells located in the upper chamber were extracted using a cotton swab. Under a microscope, the invasive cells attached to the lower membrane surface were meticulously fixed, stained, and enumerated in five randomly selected fields of view.

In vivo tumor formation experiments in nude mice: Six- to 8-week-old male nude mice were obtained from Hefei Qingyuan Biotechnology Co., Ltd. and housed under specific pathogen-free (SPF) conditions. LUAD cells (5×10^6) stably transfected with shPSMA4 or shControl were subcutaneously injected into the axillary region of nude mice (n = 5 per group). Tumor volume was measured twice each week by using the following formula: volume (mm^3) = 0.5 × length × $width^2$. After 30 days, we euthanized the mice, anesthetizing each one with pentobarbital sodium (0.1 ml/kg body weight) and taking photos. Then we performed cervical dislocation to kill the mice, removed the tumors and measured their weights. The mouse carcasses were placed together in an ice box for temporary storage, and then were collectively incinerated. All animal procedures were

approved by the Anhui Provincial Center for Disease Control and Prevention's Experimental Animal Welfare and Ethics Committee and were conducted in accordance with their guidelines.

Immunohistochemistry (IHC) analysis and immunofluorescence (IF) assay: Paraffin-embedded human and mouse tumor tissue sections were dewaxed, rehydrated, and subjected to antigen retrieval. Endogenous peroxidase activity was blocked with 3% hydrogen peroxide, and the sections were subsequently blocked with serum. For IHC, the sections were incubated overnight at 4°C with anti-PSMA4 primary antibody (Proteintech, Cat# 11943-2-AP, 1:200), followed by incubation with S-vision immunohistochemistry polymer secondary antibody (mouse/rabbit universal; Servicebio, Cat# G1303-10ML; ready to use, 100 µL per section). Signals were visualized using a DAB substrate, followed by hematoxylin counterstaining. The staining results were evaluated microscopically according to the intensity and proportion of positive cells. For IF, the sections were incubated overnight at 4°C with primary antibodies against PSMA4 (Proteintech, Cat# 11943-2-AP, 1:200), Ki-67 (Proteintech, Cat# 28074-1-AP, 1:300), E-cadherin (Proteintech, Cat# 20874-1-AP, 1:500), vimentin (Proteintech, Cat# 10366-1-AP, 1:500), or p53 (Proteintech, Cat# 10442-1-AP, 1:400), followed by incubation with Cy3-conjugated goat anti-rabbit IgG (Servicebio, Cat# GB21303, 1:300) or Cy3-conjugated goat anti-mouse IgG (Servicebio, Cat# GB21301, 1:300), as appropriate. Nuclei were counterstained with DAPI prior to imaging with a confocal microscope.

Co-immunoprecipitation (Co-IP) assay: The collected A549 and PC-9 cells were resuspended in 1 ml of IP lysis buffer containing 1% protease inhibitor and incubated on ice for 30 minutes. After centrifugation, the supernatants were collected, and a fraction was reserved as input. The remaining lysates were incubated overnight at 4°C with anti-PSMA4 or anti-p53 antibodies, followed by incubation with protein A/G agarose beads to precipitate the immune complexes. After washing three times with cold lysis buffer, the bound proteins were eluted by boiling in loading buffer and analyzed by Western blotting.

Ubiquitination assay: After co-transfecting the stable cell lines of A549 and PC-9 with the His-Ub and p53-Flag plasmids for 42 hours, 10 µm MG132 (proteasome inhibitor, APExBIO, Cat# A2585) was added and the cells were treated for 6 hours. After collecting the cells and extracting the proteins, they were suspended in SDS buffer diluted to a 1× SDS concentration and boiled to ensure complete protein denaturation. Ubiquitinated p53 was detected by Western blot using an anti-Flag antibody.

Cycloheximide (CHX) chase assays: The cells were treated with 10 µg/mL CHX (aladdin, Cat# C112766) to block the synthesis of new proteins. At the specified time points (0 h, 2 h, 4 h, 6 h, 8 h), the cells were collected and proteins were extracted for WB assay.

Statistical analysis

Statistical analysis was completed by GraphPad Prism 9. All quantitative results were presented as mean ± SD, $*P < 0.05$, $**P < 0.01$, $***P < 0.001$, $****P < 0.0001$, ns: non-significant, $P > 0.05$. All experiments were conducted in triplicate. Statistical comparisons between groups were conducted using unpaired or paired Student's t-test, or one-way analysis of variance (ANOVA) as appropriate for the specific experimental design and comparison being made.

Results

Data analysis results

SMR and HEIDI tests: First, the associations among gene expression, DNAm, and lung cancer were systematically explored using the SMR and HEIDI methods. To minimize interference from multiple effect factors and enhance causal inference reliability, genetic variations in cis-regulatory regions were exclusively selected as IVs. The summary analysis based on the cis-eQTL and cis-mQTL data revealed that 55 transcriptional probes (corresponding to 55 genes) were significantly associated with lung cancer at the transcriptional level (FDR < 0.05 and p_HEIDI > 0.05, **Table 3**). Moreover, at the methylation level, 313 DNAm probes (corresponding to 125 neighboring genes) showed a significant association with lung cancer (FDR < 0.05 and p_HEIDI > 0.05, **Table 3**). Notably, 13 of these genes showed significant associa-

Table 3. Summary of SMR calculation results for each GWAS dataset

Data sources	Filename	eQTL	mQTL
finngen_R10	C3_NSCLC_ADENO_EXALLC	PSMA4, HYKK	PSMA4, CHRNA3
	C3_NSCLC_SQUAM_EXALLC	PSMA4, HYKK, KIAA1614-AS1	--
	C3_BRONCHUS_LUNG_EXALLC	PSMA4, WDR61, HYKK, AMT, PDCD6IP, TCTA, NICN1, POC1A, PROB1, SPATA24, SKIC8, DNAJA4, QRICH1	WDR6, DALRD3, KLHDC8B, TCTA, RHOA, BSN, RHOA, CLPTM1L, SLC23A1, LOC389333, CHRNA5, CHRNA4
	C3_LUNG_NONSMALL_EXALLC	PSMA4, HYKK	CLPTM1L, CHRNA5
ukbb	LUNG_CANCER	PSMA4, IREB2	IREB2, CHRNA3
ieu	ukb-b-20176	PSMA4, HYKK, IRF4, HCG11, C4A, LOC110384692, CYP21A2, MAP1A, STRCP1, CATSPER2P1, PDIA3, AC011330.5, STRC	TGM7
	ukb-b-14521	PSMA4, VRK2, CLPTM1L, SEMA6A-AS1, ZSCAN16, ZKSCAN4, ZNF311, HLA-K, HLA-E, SKIC2, C4B....	PSMA4, CAMTA1, PTPRF, KDM4A, PIK3C2B, MDM4, ESPNL, SCLY, BSN, UROC1, ZAR1, TERT, CLPTM1L....
	ieu_b_4955	PSMA4, HYKK, IREB2	PSMA4, CLPTM1L, IREB2

Note: Abbreviations: SMR, Summary-Data-Based Mendelian Randomization; GWAS, genome-wide association studies; eQTL, expression quantitative trait locus; mQTL, methylation quantitative trait locus.

tions with lung cancer at both transcriptional and DNAm levels. The analysis results of different GWAS datasets are shown in **Figures 2A-H**, S1 and Tables S1, S2, S3, S4, S5, S6, S7, S8. Importantly, the SMR analysis results of the "ukb-b-14521" dataset are relatively comprehensive, and the precise data are provided in Table S9.

Trajectory visualization analysis: By integrating the analysis results of eQTL-GWAS SMR and mQTL-GWAS SMR (through selection of the intersection), we identified 13 genes exhibiting a significant association with lung cancer, namely *PSMA4*, *TCTA*, *IREB2*, *CLPTM1L*, *ZKSCAN4*, *HLA-E*, *HLA-DQB1*, *HLA-J*, *CYP21A2*, *TAPBP*, *MDM4*, *NEU1*, and *B3GALT4*. **Table 4** shows the specific GWAS and QTL data corresponding to these genes. Of these 13 genes, we excluded *IREB2*, *CLPTM1L*, *HLA-E*, and *CYP21A2* as their relationship with lung cancer is previously established and *MDM4*, *NEU1*, and *B3GALT4* genes as they lack corresponding transcriptome data in the SMR Portal database. For the remaining candidate genes, we conducted multi-omics trajectory visualization analysis (parameter settings: p_SMR = 1e-05, p_HEIDI = 0.05). The results showed revealed that the *PSMA4* gene alone displayed a significant correlation with both transcriptome and methylation groups, and this result was consistent across multiple independent datasets (**Figure 2I-L**).

Based on SMR findings, we comprehensively characterized the relationship between PSMA4 and lung cancer through integrated DNAm and transcription analyses using LUAD GWAS data (FinnGen R10: NSCLC, adenocarcinoma, and cancer-free controls), eQTLGen data, and McRae mQTL results. A significant association was observed between the DNAm site cg04140906 and lung cancer risk, corresponding to the PSMA4 expression level. As illustrated in **Figure 2I**, the integrated analysis revealed that the methylation probe cg04140906 resides within the promoter region of PSMA4 (ENSG00000041357) across multiple cell types and tissues. Genetic proximity analysis showed that cg04140906 is located 6557 bp from the lead SNP in mQTL-GWAS analysis, while the ENSG00000041357 transcript is positioned 11,000 bp from the top SNP in eQTL-GWAS analysis. These findings suggest that genetic variants in the PSMA4 promoter region may influence the DNAm status, thereby modulating PSMA4 expression. Next, we validated this conclusion by conducting colocalization and correlation analyses.

Colocalization analysis: For the PSMA4-associated datasets summarized in **Table 4**, we performed Bayesian colocalization analysis and

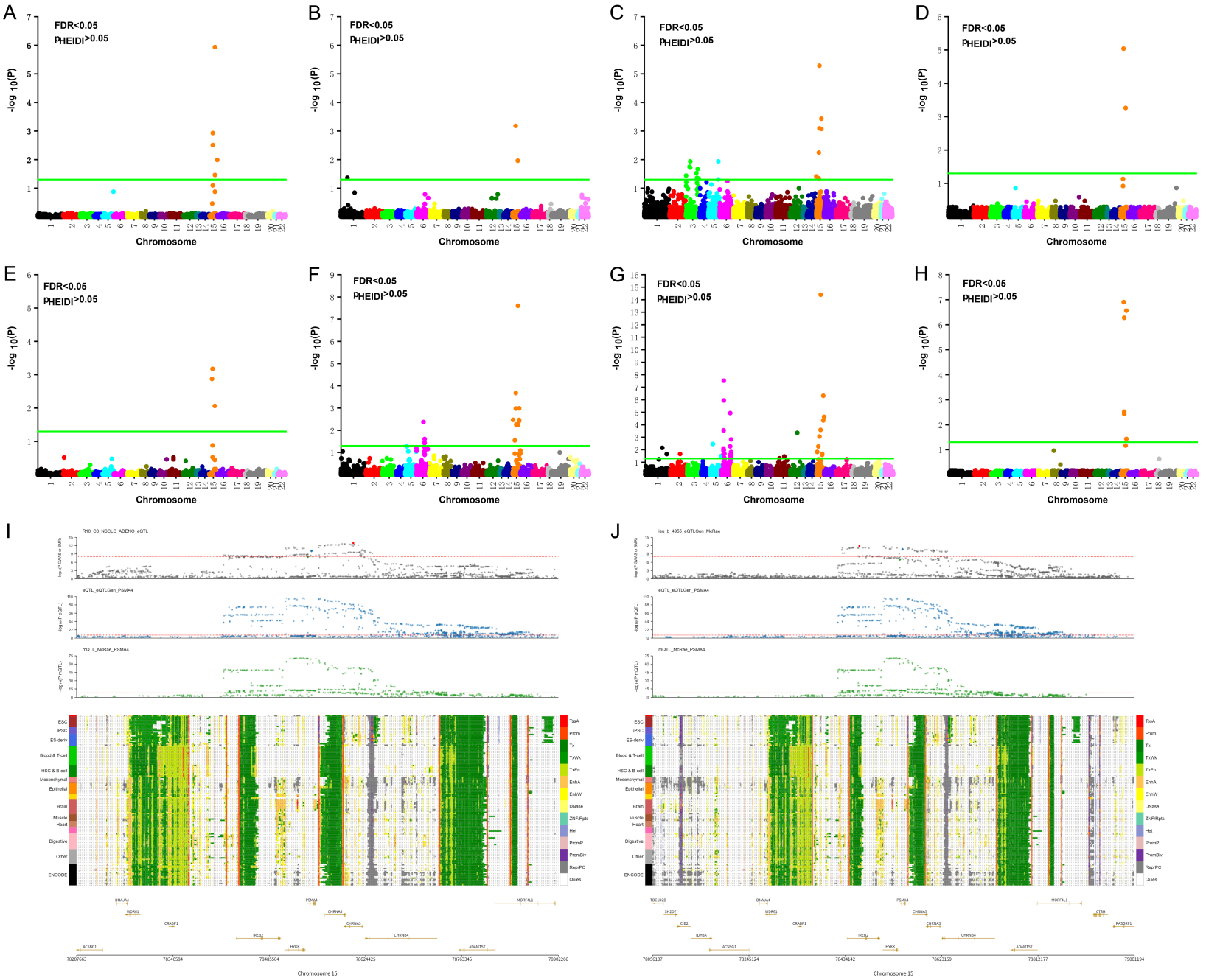
A
B
C
D
E
F
G
H
FDR<0.05
PHEIDI>0.05
-log 10(P)
Chromosome
I
J
R10_C3_NSCLC_ADENO_eQTL
eQTL_eQTLGen_PSMA4
mQTL_McRae_PSMA4
ieu_b_4955_eQTLGen_McRae
ESC
iPSC
ES-derv
Blood & T-cell
HSC & B-cell
Mesenchymal
Epithelial
Brain
Muscle
Heart
Digestive
Other
ENCODE
TssA
Prom
Tx
TxWk
TxEn
EnhA
EnhW
DNase
ZNF/Rpts
Het
PromP
PromBiv
ReprPC
Quies
Chromosome 15

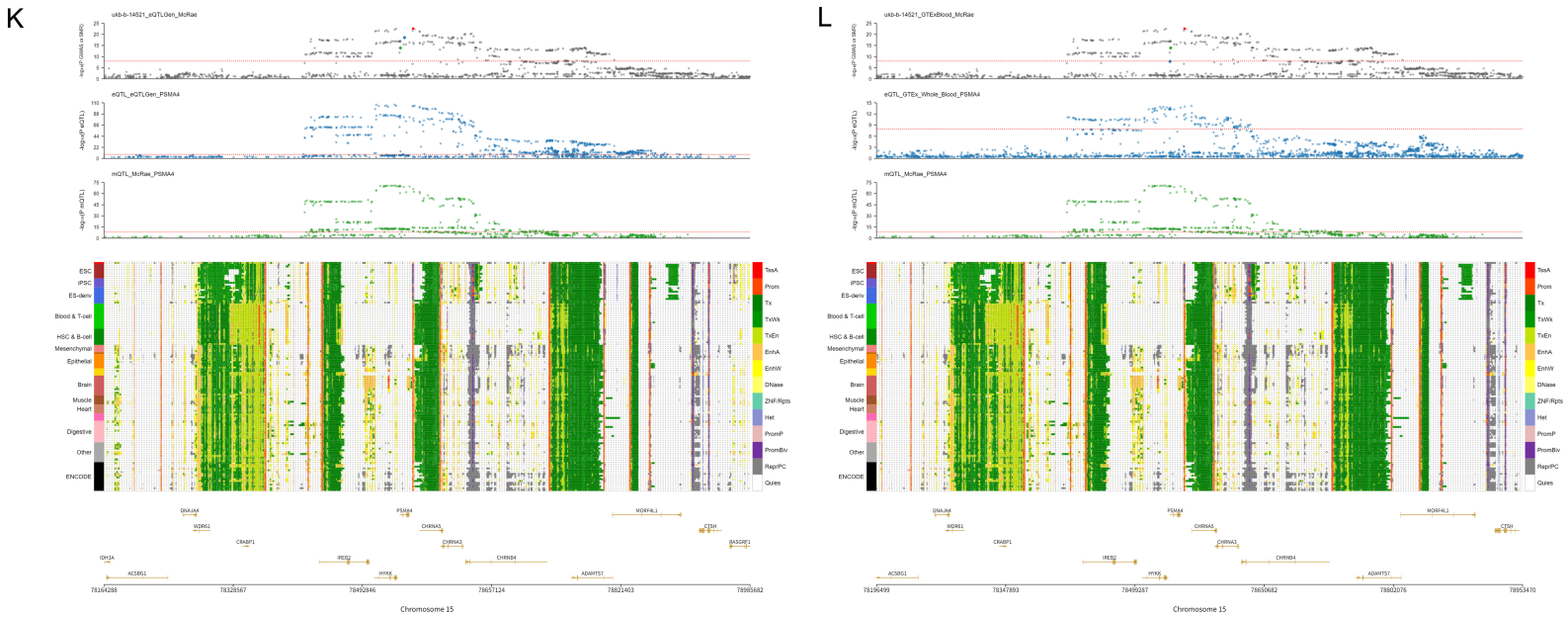

Figure 2. SMR results across multiple GWAS datasets and Trajectory visualization of PSMA4 in lung cancer. (A-H) Manhattan plots of significant results from summary data-based Mendelian randomization in overall lung cancer. (A-H) represent the aggregated results of SMR calculations conducted separately by each GWAS dataset (finngen_R10:C3_NSCLC_ADENO_EXALLC, C3_NSCLC_SQUAM_EXALLC, C3_BRONCHUS_LUNG_EXALLC, C3_LUNG_NONSMALL_EXALLC, ukbb: LUNG_CANCER, ieu: ukb-b-20176, ukb-b-14521, ieu_b_4955) with different eQTL datasets(QTLGen, GTEx_Blood, GTEx_Lung, CAGE, Westra). The green solid line indicates *P*-value threshold after false discovery rate is 0.05, FDR < 0.05, p_HEIDI > 0.05. (I-L): The omics SMR plots of PSMA4 in different datasets. (I) shows the omics SMR plots of PSMA4 in the finngen_R10:C3_NSCLC_ADENO_EXALLC, QTLGen, and McRae datasets. (J) shows the omics SMR plots of PSMA4 in the ieu:ieu_b_4955, QTLGen and McRae datasets. (K) shows the omics SMR plots of PSMA4 in the ieu: ukb-b-14521, QTLGen and McRae datasets. (L) shows the omics SMR plots of PSMA4 in the ieu: ukb-b-14521, GTExBlood and McRae datasets. Each gray solid dot represents a SNP in the GWAS data, each blue solid dot represents a SNP in the eQTL data, each green solid dot represents a SNP in the mQTL data, the red dot represents the top SNP, the blue diamond represents the transcriptome probe site, the green diamond represents the methylation probe site, and the red line represents the pSMR threshold of 5e-08. Abbreviations: SMR, summary data-based Mendelian randomization; GWAS, the genome-wide association study; SNPs, single nucleotide polymorphisms; eQTL, expression quantitative trait loci; mQTL, methylation Quantitative Trait Loci; FDR, false discovery rate; HEIDI test, heterogeneity in dependent instruments test.

Table 4. The 13 intersecting genes obtained from the SMR analysis correspond to the respective databases

Data sources	GWAS	eQTL	mQTL	Intersection gene
finngen_R10	C3_NSCLC_ADENO_EXALLC	QTLGen	McRae	PSMA4
		GTEx_Blood		
		Westra		
	C3_BRONCHUS_LUNG_EXALLC	QTLGen	McRae	TCTA
ukbb	LUNG_CANCER	CAGE	McRae	IREB2
		Westra		
ieu	ukb-b-14521	QTLGen	McRae	PSMA4, CLPTM1L, ZKSCAN4, HLA-E, HLA-DQB1
		GTEx_Blood		PSMA4, HLA-J, CYP21A2, TAPBP
		GTEx_Lung		HLA-J
		CAGE		MDM4, NEU1, B3GALT4
		Westra		PSMA4, MDM4
	ieu_b_4955	QTLGen	McRae	PSMA4
		CAGE		IREB2
		Westra		PSMA4, IREB2

Note: Abbreviations: SMR, Summary-Data-Based Mendelian Randomization; GWAS, genome-wide association studies; eQTL, expression quantitative trait locus; mQTL, methylation quantitative trait locus.

generated corresponding correlation plots. Because the GTEx_Blood and Westra eQTL datasets lack effect allele frequency information, colocalization analysis was separately conducted between the GWAS datasets (FinnGen_R10:C3_NSCLC_ADENO_EXALLC, ieu:ukb-b-14521, and ieu_b_4955) and the QTLGen data (**Figure 3**). As depicted in **Figure 3A**, PSMA4 expression exhibited a positive correlation with LUAD development, whereas PSMA4 methylation showed a negative association with tumor occurrence. Furthermore, an inverse association was observed between PSMA4 expression and its methylation level. Colocalization analysis further indicated that SNPs regulating PSMA4 expression may concurrently influence LUAD susceptibility. Consistent findings were obtained from the ukb-b-14521 (PP.H4 = 0.786) and ieu_b_4955 (PP.H4 = 0.99) datasets (**Figure 3B**, **3C**). Based on these trajectory visualization results, we propose a mechanistic hypothesis: elevated PSMA4 expression increases lung cancer risk, whereas genetic variations in the PSMA4 promoter region induce DNAm - potentially by disrupting transcription factor binding - thereby downregulating PSMA4 expression and reducing lung cancer risk. Additionally, PSMA4 appears to exhibit a stronger disease-specific association with LUAD.

We further analyzed the association of MDM4, NEU1, and B3GALT4 with lung cancer risk through correlation and colocalization tests. Among these candidates, B3GALT4 alone demonstrated significant colocalization evidence (Figure S2). Both transcription expression and methylation levels of B3GALT4 were positively associated with lung cancer development. A noteworthy finding is a clear link between the expression pattern of the genes and their methylation status. Colocalization analysis further indicated that genetic variants regulating B3GALT4 expression may simultaneously influence LUAD susceptibility, as supported by a PP.H4 value of 0.85. These findings suggest that B3GALT4 may also be a potential therapeutic target associated with lung carcinogenesis.

Bulk RNA-seq analysis and online database validation

From the GEO database, we selected the LUAD RNA-seq dataset GSE159857 involving only European subjects (specific grouping information is shown in Table S10). A differential expression analysis of the transcriptome genes screened by SMR (**Figure 4A-C**; full results in Table S11) revealed that among the 55 transcriptome genes in GSE159857, 9 genes were significantly upregulated, 3 genes were significantly downregulated, and 28 genes had a stable expression level. Notably, PSMA4 was significantly overexpressed ($P < 0.05$), whereas B3GALT4 expression remained intact. These

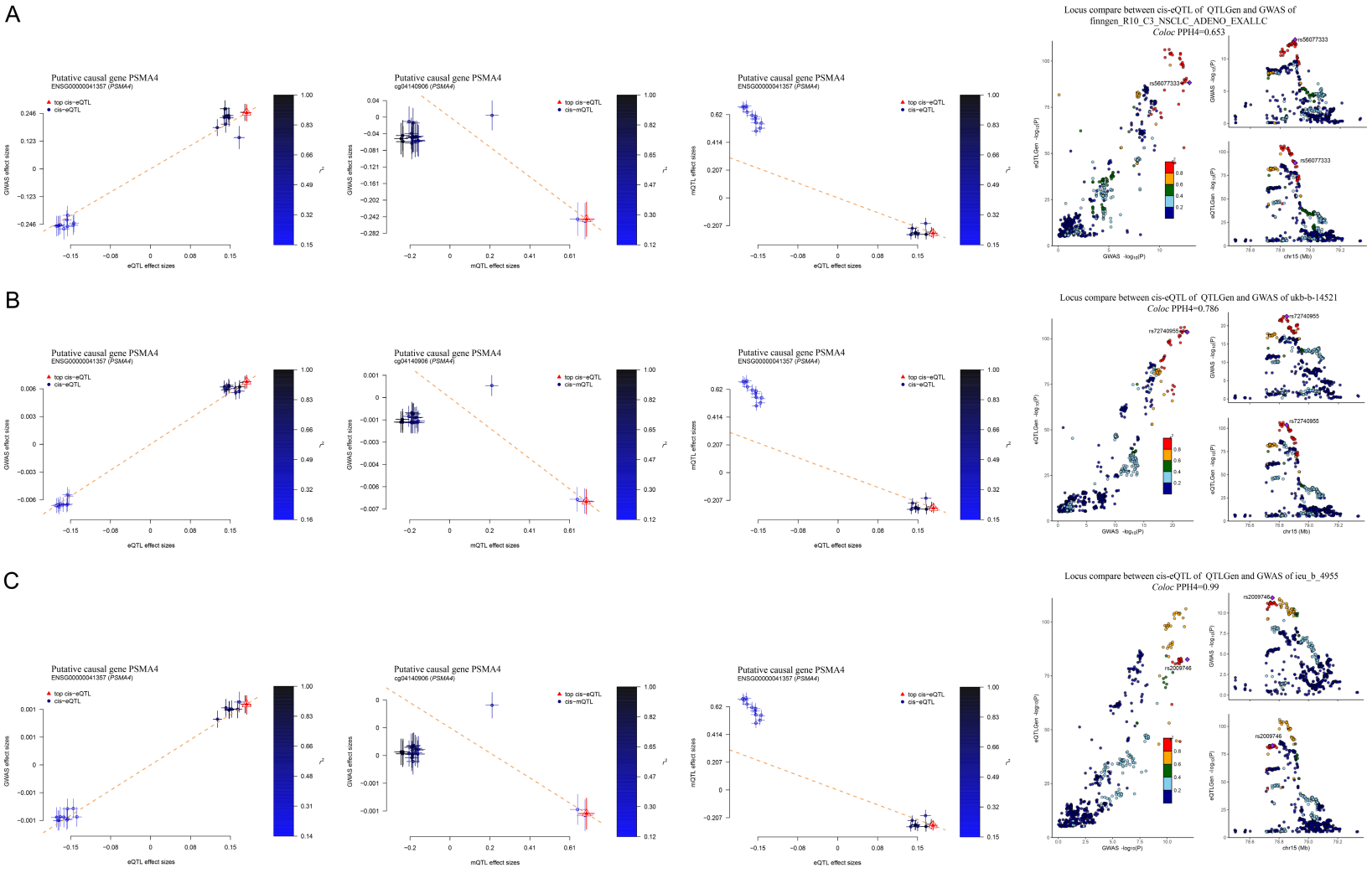

Figure 3. Based on the results of SMR, a correlation analysis and co-localization analysis were conducted between the GWAS datasets and the QTL datasets corresponding to PSMA4. (A) shows the correlation analysis and colocalization analysis results of the GWAS dataset of finngen_R10:C3_NSCLC_ADENO_EXALLC with the eQTL dataset of QTLGen and the mQTL dataset of McRae. From left to right, they are the correlation diagrams of eQTL-GWAS, mQTL-GWAS, eQTL-mQTL, and colocalization analyses. (B) shows the correlation analysis and colocalization analysis results of the GWAS dataset of ieu: ukb-b-14521 with the eQTL dataset of QTLGen and the mQTL dataset of McRae. From left to right, they are the correlation diagrams of eQTL-GWAS, mQTL-GWAS, eQTL-mQTL, and colocalization analyses. (C) shows the correlation analysis and colocalization analysis results of the GWAS dataset of ieu:ieu_b_4955 with the eQTL dataset of QTLGen and the mQTL dataset of McRae. From left to right, they are the correlation diagrams of eQTL-GWAS, mQTL-GWAS, eQTL-mQTL, and colocalization analyses. Abbreviations: SMR, summary data-based Mendelian randomization; GWAS, the genome-wide association study; SNPs, single nucleotide polymorphisms; eQTL, expression quantitative trait loci; mQTL, methylation Quantitative Trait Loci; PP.H4, the posterior probability of hypothesis 4.

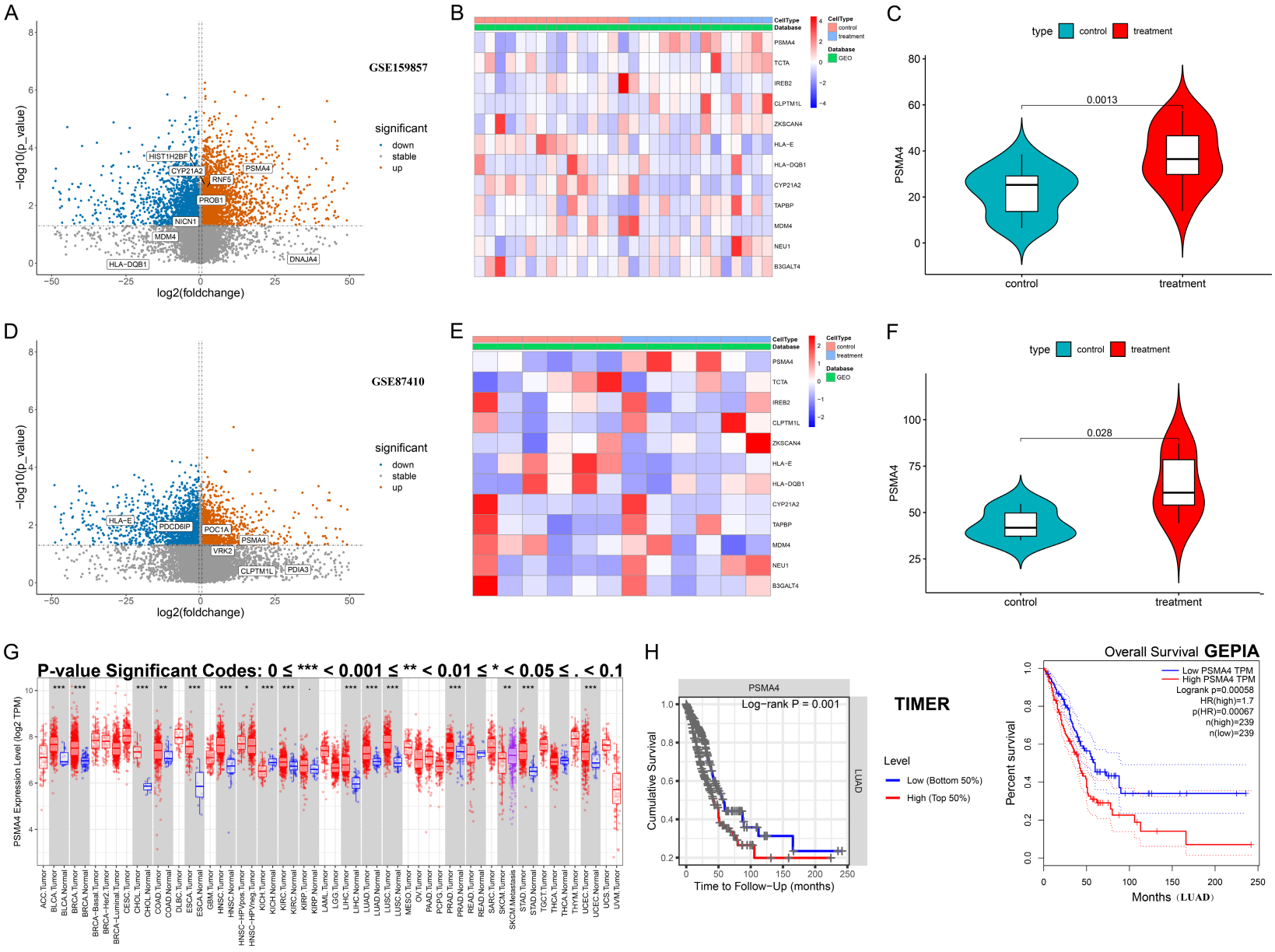
A
GSE159857
significant
down
stable
up
−log10(p_value)
log2(foldchange)
HIST1H2BF
CYP21A2
RNF5
PSMA4
PROB1
NICN1
MDM4
HLA−DQB1
DNAJA4
B
CellType
Database
control
treatment
GEO
PSMA4
TCTA
IREB2
CLPTM1L
ZKSCAN4
HLA−E
HLA−DQB1
CYP21A2
TAPBP
MDM4
NEU1
B3GALT4
C
type
control
treatment
PSMA4
0.0013
control
treatment
D
GSE87410
significant
down
stable
up
−log10(p_value)
log2(foldchange)
HLA−E
PDCD6IP
POC1A
PSMA4
VRK2
CLPTM1L
PDIA3
E
CellType
Database
control
treatment
GEO
PSMA4
TCTA
IREB2
CLPTM1L
ZKSCAN4
HLA−E
HLA−DQB1
CYP21A2
TAPBP
MDM4
NEU1
B3GALT4
F
type
control
treatment
PSMA4
0.028
control
treatment
G
P-value Significant Codes: 0 ≤ *** < 0.001 ≤ ** < 0.01 ≤ * < 0.05 ≤ . < 0.1
PSMA4 Expression Level (log2 TPM)
ACC.Tumor
BLCA.Tumor
BLCA.Normal
BRCA.Tumor
BRCA.Normal
BRCA−Basal.Tumor
BRCA−Her2.Tumor
BRCA−Luminal.Tumor
CESC.Tumor
CHOL.Tumor
CHOL.Normal
COAD.Tumor
COAD.Normal
DLBC.Tumor
ESCA.Tumor
ESCA.Normal
GBM.Tumor
HNSC.Tumor
HNSC.Normal
HNSC−HPVpos.Tumor
HNSC−HPVneg.Tumor
KICH.Tumor
KICH.Normal
KIRC.Tumor
KIRC.Normal
KIRP.Tumor
KIRP.Normal
LAML.Tumor
LGG.Tumor
LIHC.Tumor
LIHC.Normal
LUAD.Tumor
LUAD.Normal
LUSC.Tumor
LUSC.Normal
MESO.Tumor
OV.Tumor
PAAD.Tumor
PCPG.Tumor
PRAD.Tumor
PRAD.Normal
READ.Tumor
READ.Normal
SARC.Tumor
SKCM.Tumor
SKCM.Metastasis
STAD.Tumor
STAD.Normal
TGCT.Tumor
THCA.Tumor
THCA.Normal
THYM.Tumor
UCEC.Tumor
UCEC.Normal
UCS.Tumor
UVM.Tumor
H
PSMA4
Log−rank P = 0.001
Cumulative Survival
Time to Follow−Up (months)
LUAD
TIMER
Level
Low (Bottom 50%)
High (Top 50%)
Overall Survival GEPIA
Low PSMA4 TPM
High PSMA4 TPM
Logrank p=0.00058
HR(high)=1.7
p(HR)=0.00067
n(high)=239
n(low)=239
Percent survival
Months (LUAD)

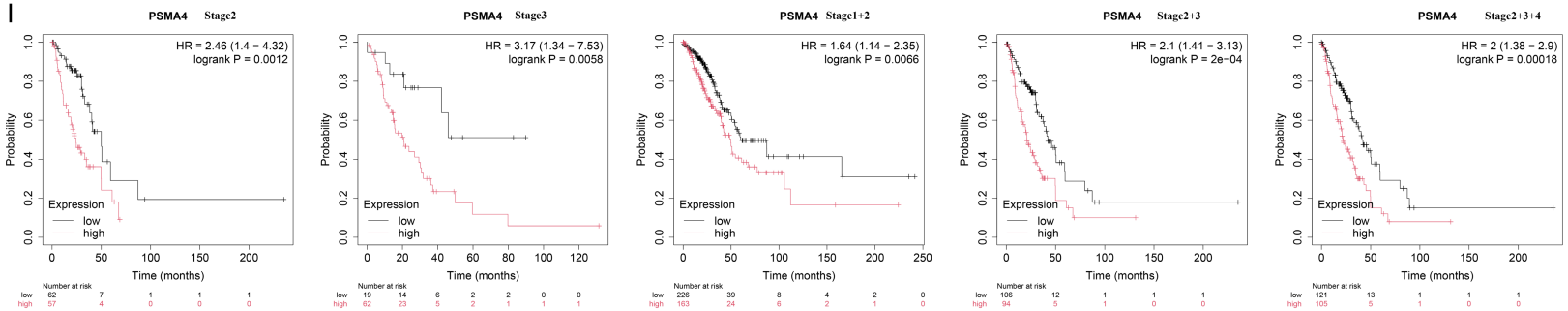

Figure 4. The combination diagram of bulk RNA-seq analysis and the verification results of the online database. A. The volcano map of differential gene analysis in the GSE159857 dataset, blue represents down-regulated gene, orange represents up-regulated gene, and gray represents no significant gene; B. Heat map of differential gene analysis in the GSE159857 dataset; C. The expression of PSMA4 in the GSE159857 dataset; D. The volcano map of differential gene analysis in the GSE87410 dataset, blue represents down-regulated gene, orange represents up-regulated gene, and gray represents no significant gene; E. Heat map of differential gene analysis in the GSE87410 dataset; F. The expression of PSMA4 in the GSE87410 dataset; G. The differential expression of PSMA4 in the TIMER database; H. The survival analysis curve of PSMA4 in the TIMER database and GEPIA database; I. Survival analysis curve of PSMA4 in patients at different stages in Kaplan-Meier Ploter. Abbreviations: RNA-seq, RNA sequencing; GEPIA, Gene Expression Profiling Interactive Analysis.

findings were further validated in an independent Asian cohort (GSE87410; Table S10), where 3 genes were upregulated, 2 genes were downregulated, and 35 genes exhibited a stable expression level (**Figure 4D-F**; Table S12). Consistent with the European dataset, PSMA4 was significantly overexpressed ($P < 0.05$), while B3GALT4 showed no differential expression; this finding confirmed the reproducibility of PSMA4 association with lung cancer risk across ethnic populations.

By conducting an integrated analysis with TIMER and GEPIA databases, we evaluated both the expression patterns and prognostic significance of PSMA4 in LUAD. TIMER analysis confirmed PSMA4 overexpression in tumor tissues ($P < 0.05$; **Figure 4G**). Consistent survival assessments from both platforms demonstrated that patients with elevated PSMA4 levels had significantly shorter OS than those with low PSMA4 levels ($P < 0.05$; **Figure 4H**). Further validation with the Kaplan-Meier Plotter revealed stage-specific prognostic impact: across stages II, III, II + III, and II + III + IV of LUAD, high PSMA4 expression was consistently correlated with reduced patient survival ($P < 0.05$; **Figure 4I**). Collectively, these results establish that PSMA4 is significantly associated with LUAD progression, and its elevated expression appears to promote disease development.

PPI evaluation

To map the functional interactions of SMR-identified candidates and the currently known lung cancer-related targets, we constructed a PPI network using the STRING database with the interaction significance threshold set to $P < 0.05$ (Figure S3). The obtained network was imported into Cytoscape (v3.10.3) for visualization and topology analysis. Each node's importance was measured using the Betweenness Centrality (BC) metric (**Figure 5** and Table S13). PSMA4 exhibited a high BC value, ranking 13th among all nodes, including the established lung cancer targets; this finding indicates the central role of PSMA4 in the network. It significantly interacts with multiple core oncoproteins, including TP53, TNF, AKT1, NF1, CD274, EGFR, RPS18, KRAS, and TERT. Notably, PSMA4 showed the strongest association with TP53, and its high ranking among previously validated targets highlights its potential functional importance in LUAD pathogenesis.

Experimental results

PSMA4 is highly expressed in LUAD tissues and cell lines: We conducted immunohistochemical staining on 10 pairs of LUAD samples to assess the expression level of PSMA4. The detailed clinical and pathological characteristics of the patient are presented in Table S14. We performed semi-quantitative evaluation of PSMA4 expression using the H-score method and found that the expression of PSMA4 in lung adenocarcinoma tissues was significantly higher compared to the matched normal tissues (**Figure 6A**, **6B**). Complementary WB assays demonstrated consistent upregulation of PSMA4 expression across multiple lung cancer cell lines, with A549 and PC-9 cells showing the highest expression levels among the six tested lines; moreover, the PSMA4 expression levels in all these cells lines exceeded that observed in normal BEAS-2B cells (**Figure 6C**, **6D**).

PSMA4 promotes the growth, proliferation, and invasion of LUAD cells: To investigate the role of PSMA4 in LUAD malignancy, we established stable KD and OE cell lines through lentiviral transduction. qPCR analysis and WB assay confirmed effective PSMA4 suppression with shRNA constructs, with shPSMA4-2 and shPSMA4-3 demonstrating the most prominent reduction in both mRNA (Figure S4A, S4D) and protein levels (Figure S4B, S4C, S4E, S4F) in A549 and PC-9 cells, shPSMA4-2 and shPSMA4-3 were selected for functional assays based on their superior knockdown efficiency at both mRNA and protein levels. Conversely, PSMA4-overexpressing A549 cells exhibited significant upregulation at both transcriptional (Figure S4G) and translational levels (Figure S4H, S4I). Functional assessment with CCK-8 and EdU assays revealed that PSMA4 KD impaired the viability of LUAD cells, whereas its OE enhanced the cells' proliferative capacity (**Figure 6E-L**).

Colony formation assay demonstrated that PSMA4 KD substantially impaired the clonogenic capacity of LUAD cells (**Figure 7A**), whereas PSMA4 OE significantly enhanced this ability in A549 cells (**Figure 7B**). These results substantiate the role of PSMA4 as an oncogene that promotes LUAD cell proliferation.

Wound healing assay also showed that PSMA4 KD markedly impaired the migratory capacity

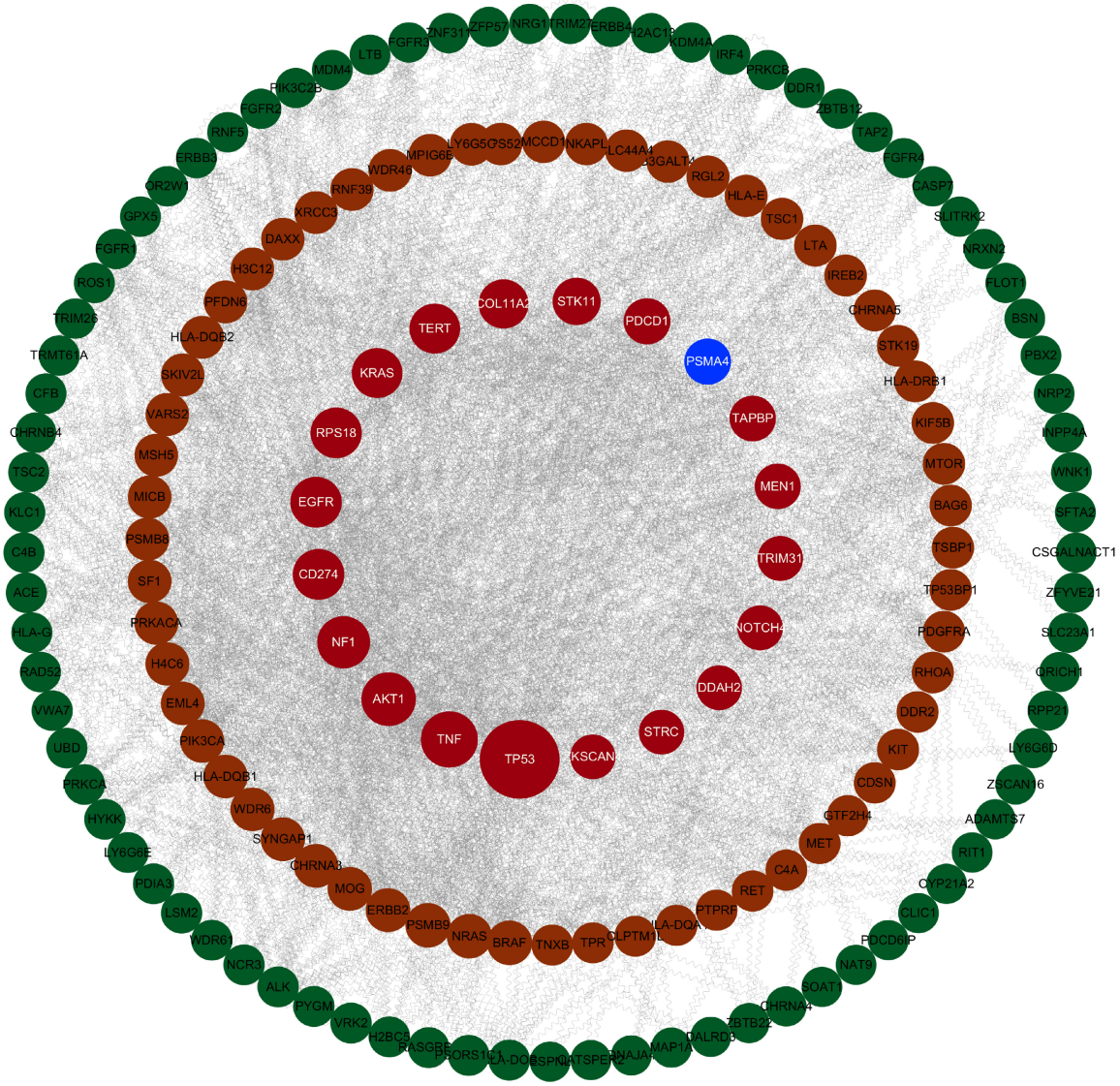

Figure 5. PPI network diagram (sorted by BC value), the size of the circles represents the BC value. Abbreviations: PPI, protein-protein interaction; BC, Betweenness Centrality.

of A549 and PC-9 cells (**Figure 7C**), whereas PSMA4 OE enhanced this ability in A549 cells (**Figure 7D**). Consistent with these findings, Transwell invasion assays revealed that PSMA4 depletion suppressed cellular invasion (**Figure 7E**, **7F**), whereas PSMA4 OE promoted the cell's invasive potential (**Figure 7G**). Collectively, these results establish PSMA4 as an oncogenic driver that facilitates both migration and invasion of LUAD cells.

PSMA4 KD inhibits LUAD cell growth in vivo: To validate the oncogenic function of PSMA4 *in vivo*, control and PSMA4-KD A549 cells were subcutaneously implanted into nude mice (**Figure 8A**). PSMA4 depletion substantially reduced tumor growth and tumor mass size (**Figure 8B**, **8C**). IF assay confirmed successful PSMA4 knockdown in the experimental group (**Figure 8D**). Concomitant molecular analyses of PSMA4-deficient tumors revealed downregulation of the proliferation marker Ki-67 and the mesenchymal marker vimentin and upregulation of the epithelial marker E-cadherin (**Figure 8E-G**), which indicated attenuated cell proliferation and a reversal of epithelial-mesenchymal transition. These *in vivo* experimental findings, consistent with our *in vitro* experimental data, establish that PSMA4 is critical for LUAD growth and progression.

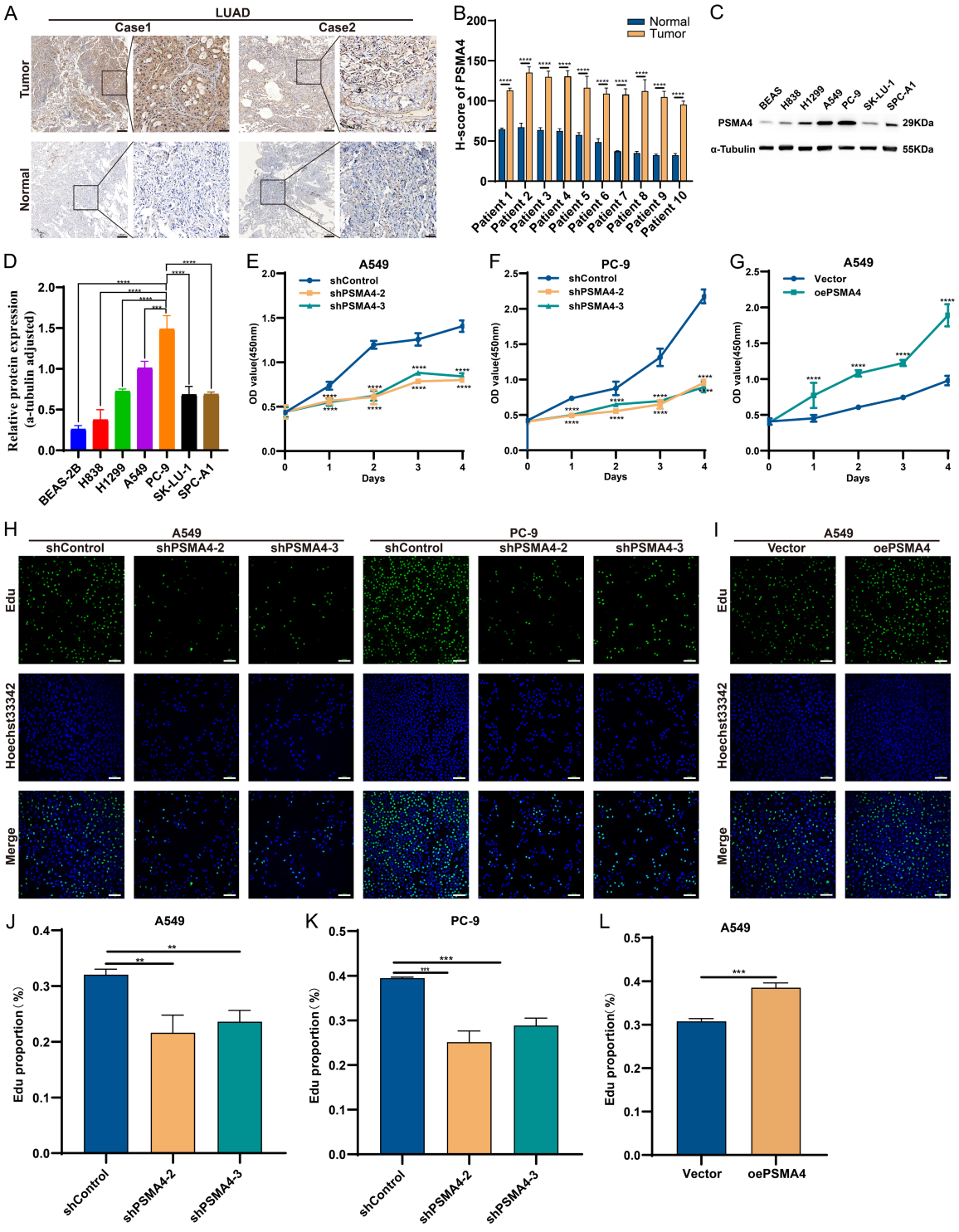

Figure 6. PSMA4 is highly expressed in LUAD tissues and promotes LUAD cell proliferation. (A) Representative images of PSMA4 expression in LUAD and adjacent normal tissues determined by IHC staining. Original magnification, 50× (left) or 200× (right). Scale (left) = 200 μm, Scale (right) = 50 μm. (B) Comparison of the H-score of PSMA4 in the IHC staining results of 10 pairs of samples, with three sights recorded for each sample. Statistical comparisons were made using a paired two-tailed Student's t-test; $^{**}P < 0.01$, $^{***}P < 0.001$, $^{****}P < 0.0001$. (C, D) Western blotting analysis of the PSMA4 protein expression levels in one normal lung cell lines (BEAS-2B) and six NSCLC cell lines. Data is presented as the mean ± SD ($^{**}P < 0.01$, $^{***}P < 0.001$, $^{****}P < 0.0001$ by *One-way ANOVA*). (E-G) CCK-8 assay analysis of the impact of PSMA4 knockdown (E, F) or overexpression (G) on LUAD cell growth. shControl:

shRNA control, shPSMA4-2: shRNA2 targeting PSMA4, shPSMA4-3: shRNA3 targeting PSMA4. Vector: Control for overexpression, oePSMA4-2: Lentivirus targeting PSMA4 for overexpression. Data is presented as the mean ± SD (**P < 0.01, ***P < 0.001, **** P < 0.0001 by repeated measures ANOVA). (H-L) The effect of PSMA4 knockdown (H) or overexpression (I) on the growth of LUAD cells was detected using EdU assay. Original magnification, 200×, Scale = 100 μm. Data is presented as the mean ± SD (**P < 0.01, ***P < 0.001, ****P < 0.0001, (J and K) were analyzed using *One-way ANOVA*, while (L) were analyzed using unpaired Student's *t*-test). Abbreviations: LUAD, lung adenocarcinoma; H-score, Histochemistry score; IHC, immunohistochemistry; CCK-8, Cell Counting Kit-8; EdU, 5-Ethynyl-2'-deoxyuridine.

GO and KEGG enrichment analysis: We performed a transcriptome sequencing analysis using PSMA4 KD cell lines. GO enrichment analysis revealed that, in the biological process category, PSMA4 primarily promoted ribosome biogenesis (GO:0042254) but predominantly inhibited fatty acid beta-oxidation (GO:0006635) and catabolism of fatty acids (GO:0009062). In the cellular component category, PSMA4 was primarily associated with ribosomal and mitochondrial functions; it positively regulated the preribosome (GO:0030684) and the mitochondrial inner membrane (GO:0005743) and negatively regulated the peroxisome (GO:0005777). In the molecular function category, PSMA4 promoted ribonucleoprotein complex binding (GO:0043021) and ribosome binding (GO:0043022) and inhibited guanyl-nucleotide exchange factor activity (GO:0005085) and GTPase activator activity (GO:0005096) (**Figure 9A**, **9B**).

The KEGG pathway enrichment analysis (**Figure 9C**) showed that PSMA4 was associated with ubiquitin-mediated proteolysis (hsa04120) and also exhibited a high degree of correlation with the p53 signaling pathway (hsa04115); this finding is consistent with the earlier reported PPI results.

PSMA4 promotes LUAD cell proliferation by inhibiting the p53 pathway: To confirm that PSMA4 influences the p53 pathway, we performed WB assay to detect p53 pathway-related proteins. PSMA4 KD increased p53 and p21 expression levels in A549 and PC-9 cells (**Figure 9D**), whereas PSMA4 OE had an opposite effect on the expression of these proteins in A549 cells (**Figure 9E**). Additionally, immunofluorescence confirmed that p53 expression was upregulated in PSMA4-knockdown nude mouse tumors compared to the control group (**Figure 9F**, **9G**). Furthermore, Western blotting revealed increased levels of p53 and p21 in PSMA4-knockdown tumors in nude mice (**Figure 9H**, **9I**). Therefore, these findings suggest that PSMA4 promotes LUAD cell proliferation by suppressing the p53 pathway. This result validated the accuracy of the PPI analysis and sequencing results.

PSMA4 facilitates proteasome-dependent turnover of ubiquitinated p53: To further clarify how PSMA4 regulates the p53 pathway, we investigated whether PSMA4 affects p53 protein turnover through the ubiquitin-proteasome system. Co-IP assays showed that PSMA4 physically interacted with p53 (**Figure 10A**). In addition, IF staining demonstrated that PSMA4 and p53 were predominantly co-localized in the nucleus (**Figure 10B**), supporting a spatial basis for their functional interaction. We next examined the ubiquitination status of p53. PSMA4 knockdown increased the abundance of ubiquitinated p53, whereas PSMA4 overexpression reduced the abundance of ubiquitinated p53 (**Figure 10C**, **10D**). Given the proteasomal role of PSMA4, these findings likely reflect altered turnover of ubiquitinated p53 rather than direct regulation of the ubiquitination reaction itself. To determine whether PSMA4-mediated regulation of p53 is proteasome-dependent, cells were treated with the proteasome inhibitor MG132 (10 μm). In PSMA4-knockdown A549 cells, p53 protein levels were significantly higher than those in control cells and were further increased after MG132 treatment (**Figure 10E**). A similar pattern was observed in PC-9 cells. Conversely, in PSMA4-overexpressing A549 cells, p53 protein levels were markedly reduced compared with those in vector control cells, whereas MG132 treatment restored p53 accumulation (**Figure 10F**). Furthermore, CHX chase assays showed that PSMA4 knockdown markedly slowed the degradation of p53 protein (**Figure 10G**), indicating that PSMA4 facilitates p53 protein turnover. Taken together, these results suggest that PSMA4 interacts with p53 and promotes the proteasome-dependent degradation of ubiquitinated p53, thereby suppressing p53 signaling.

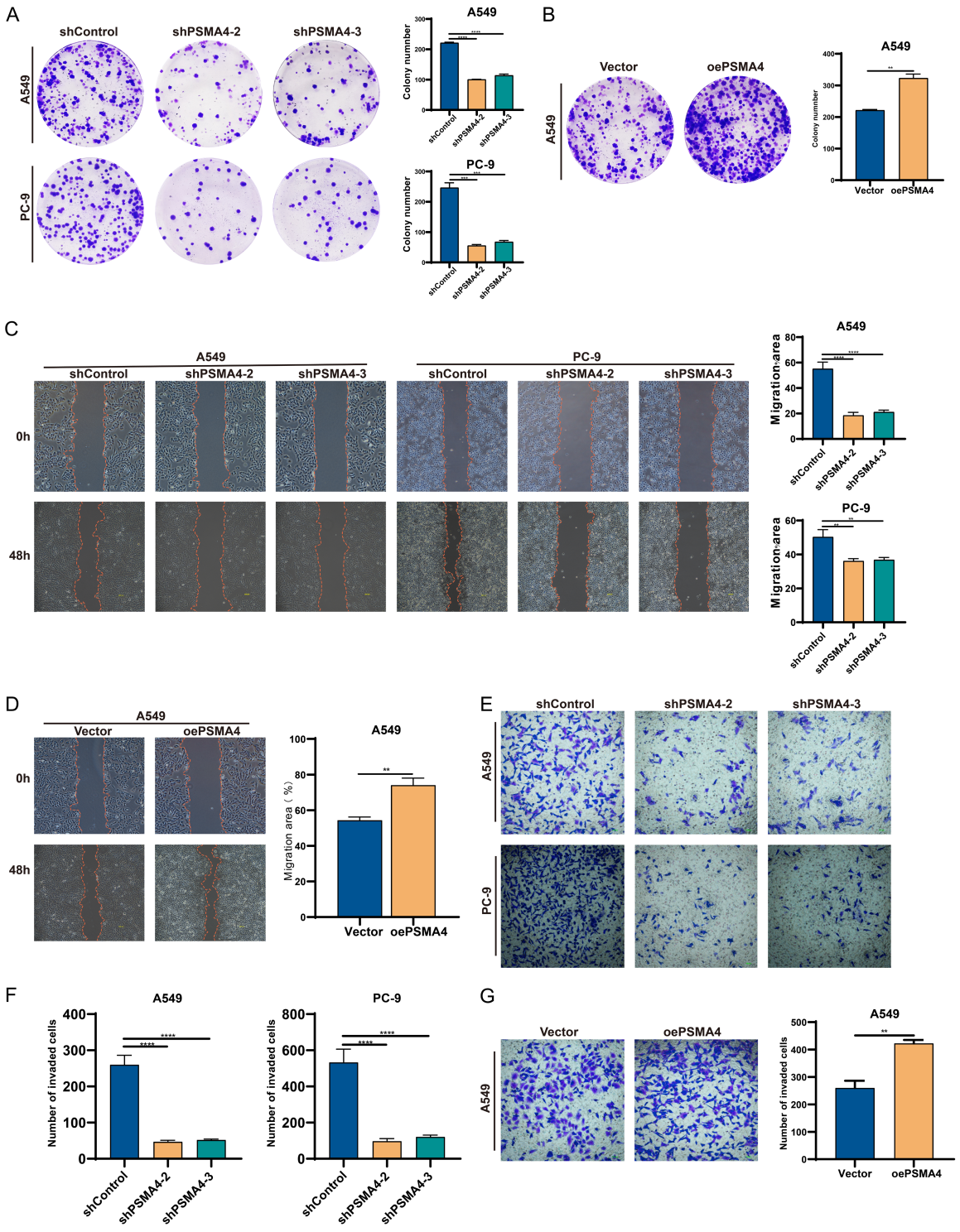

Figure 7. PSMA4 promotes the clonogenicity, migration, and invasion of LUAD cells. (A, B) Colony formation assay showing the effects of PSMA4 knockdown (A) or overexpression (B) on LUAD cell growth. (C, D) Cell scratch assay showing the effects of PSMA4 knockdown (C) or overexpression (D) on the migration ability of LUAD cells. (E-G) Transwell invasion assay showing the effects of PSMA4 knockdown (E, F) or overexpression (G) on the invasion ability of LUAD cells. Data is presented as the mean ± SD (***P* < 0.01, ****P* < 0.001, *****P* < 0.0001, (A, C and E) were analyzed using *One-way ANOVA*, while (B, D and G) were analyzed using unpaired Student's *t*-test). Abbreviations: LUAD, lung adenocarcinoma.

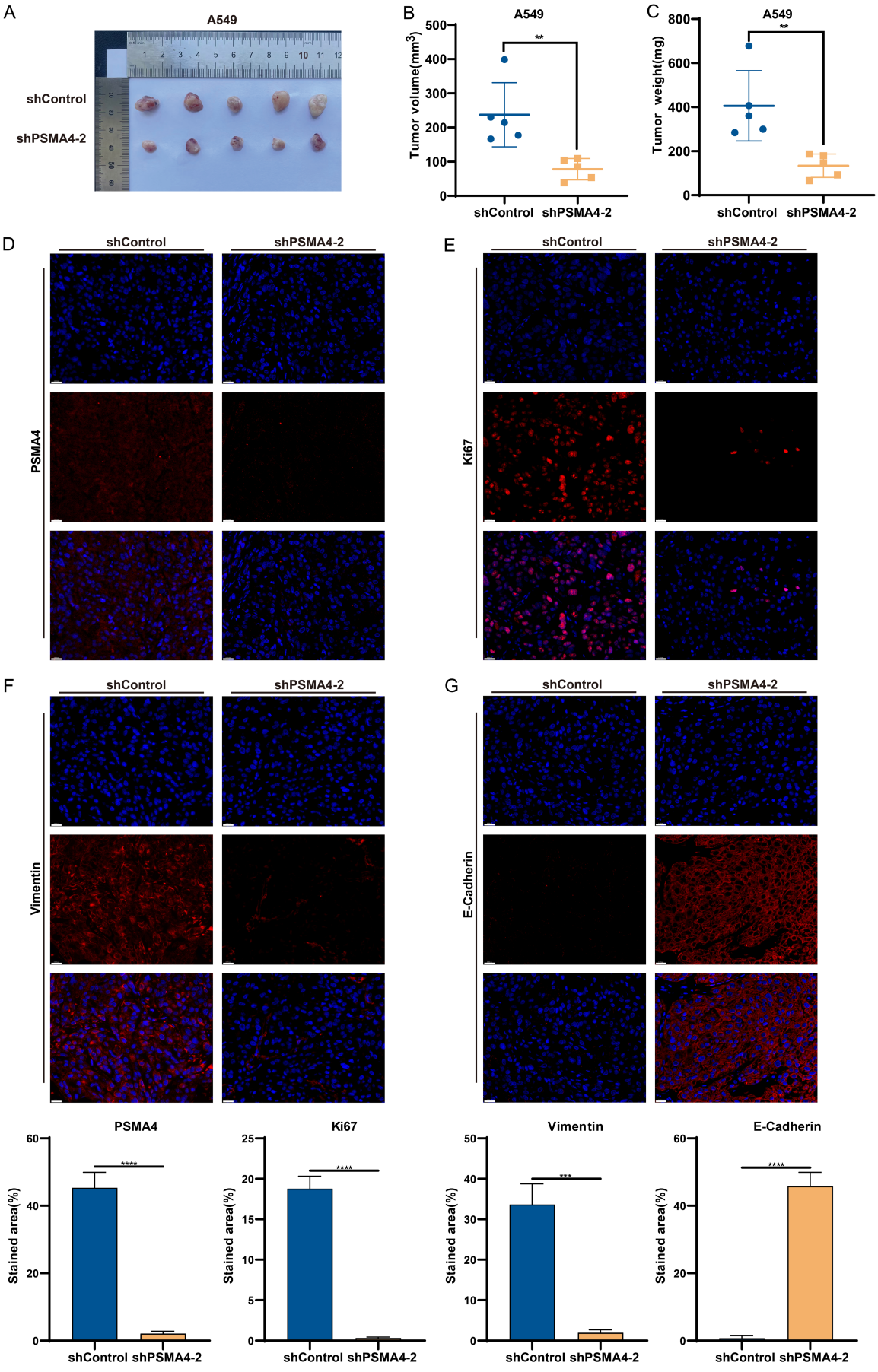
A
A549
shControl
shPSMA4-2
B
A549
Tumor volume(mm3)
shControl shPSMA4-2
C
A549
Tumor weight(mg)
shControl shPSMA4-2
D
shControl
shPSMA4-2
PSMA4
E
shControl
shPSMA4-2
Ki67
F
shControl
shPSMA4-2
Vimentin
G
shControl
shPSMA4-2
E-Cadherin
PSMA4
Ki67
Vimentin
E-Cadherin
Stained area(%)
shControl shPSMA4-2

Figure 8. PSMA4 knockdown suppresses LUAD tumor growth and EMT-related phenotypes in vivo. (A) The xenograft tumors formed in the underarm of nude mice after injection of A549 control cells (shControl) and PSMA4 knockdown cells (shPSMA4-2) on the 30th day after injection. (B, C) Measure and compare the volume sizes (B) and weights (C) of the tumors in the two groups. (D-G) IF was used to detect the expression levels of PSMA4, Ki67, Vimentin and E-Cadherin proteins in the two groups of tumors. Original magnification, 400×, Scale bar = 20 μm. Data is presented as the mean ± SD (***P* < 0.01, ****P* < 0.001, *****P* < 0.0001 by unpaired Student's *t*-test). Abbreviations: LUAD, lung adenocarcinoma; EMT, Epithelial-mesenchymal transition.

Discussion

In the present SMR study, we utilized multiple GWAS and QTL databases to screen 13 potential genes related to lung cancer (*PSMA4*, *TCTA*, *IREB2*, *CLPTM1L*, *ZKSCAN4*, *HLA-E*, *HLA-DQB1*, *HLA-J*, *CYP21A2*, *TAPBP*, *MDM4*, *NEU1*, and *B3GALT4*) from several databases. Previous studies have confirmed that *IREB2*, *CLPTM1L*, *HLA-E*, and *CYP21A2* are associated with lung cancer development, which indirectly validates the reliability of our research results. Importantly, our findings extend beyond the established association at the 15q25.1 susceptibility locus: by combining SMR with colocalization evidence, we more precisely attribute the GWAS risk signal at the gene level and prioritize PSMA4 as a leading LUAD-relevant candidate. Independent validation across GEO transcriptomic cohorts and complementary public resources further supports PSMA4's consistent dysregulation and clinical relevance, strengthening the integrative gene-level inference.

IREB2 (also known as iron response element binding protein 2, also called IRP2) is an RNA-binding protein. It controls the iron level in cells by regulating iron homeostasis-related mRNAs, especially in people with iron deficiency. Previous studies have reported that IREB2 gene variation is related to the development of lung cancer and chronic obstructive pulmonary disease (COPD) [26]. Moreover, IREB2 promotes the proliferation of lung cancer cells by regulating iron metabolism, and high-level IREB2 expression is related to tumor progression and poor prognosis [27].

The gene CLPTM1L (also called CRR9) encodes a membrane protein and plays a role in cisplatin resistance. Although CLPTM1L overexpression causes apoptosis in cisplatin-sensitive cells, it is highly expressed in cisplatin-resistant ovarian cancer cell lines [28]. Genome-wide association studies (GWAS) associate genes with the 5p15.33 locus (TERT - CLPTM1L) in lung cancer risk [29, 30]. Studies by James et al. indicate that CLPTM1L interacts with PI3K, activates AKT, up - regulates Bcl - xL, and then inhibits apoptosis of Ras - driven lung tumor cells [31].

The non-classical MHC class I molecule HLA-E belongs to important immune checkpoints. Liu et al.'s research shows that the HLA-E:CD94-NKG2A axis is involved in the interaction between circulating tumor cells (CTC) and natural killer cells (NK cells). Disrupting this pathway can enhance NK cell - mediated tumor killing in vitro and can also inhibit tumor metastasis in vivo. In addition, in pancreatic cancer models, an increase in HLA-E levels can promote liver metastasis [32]. In lung adenocarcinoma (LUAD), high expression of HLA-E is associated with lower OS, and low expression is beneficial to the survival of patients [33].

Members of the P450 superfamily encoded by CYP21A2, this member also acts as CPS1, which is the rate-limiting enzyme in the urea cycle. This enzyme is located in mitochondria and catalyzes the formation of carbamoyl phosphate from ammonia and bicarbonate to excrete nitrogenous waste. In KRAS/LKB1 mutant (KL-type) lung cancer, CYP21A2 is overactivated and also transfers mitochondrial carbamoyl phosphate to purine synthesis to provide nucleotides for tumor growth [34].

Following the exclusion of previously documented genes, we conducted trajectory visualization and colocalization analyses, which marked PSMA4 and B3GALT4 as candidate targets. These genes were subsequently evaluated using bulk RNA-seq data from European and Asian populations. PSMA4 exhibited significantly differential expression in LUAD cells in both cohorts. In contrast, B3GALT4 expression exhibited no significant alterations in both datasets. Although B3GALT4 demonstrated strong colocalization evidence, it did not exhibit consistent differential expression across independent bulk RNA-seq datasets. Therefore, within

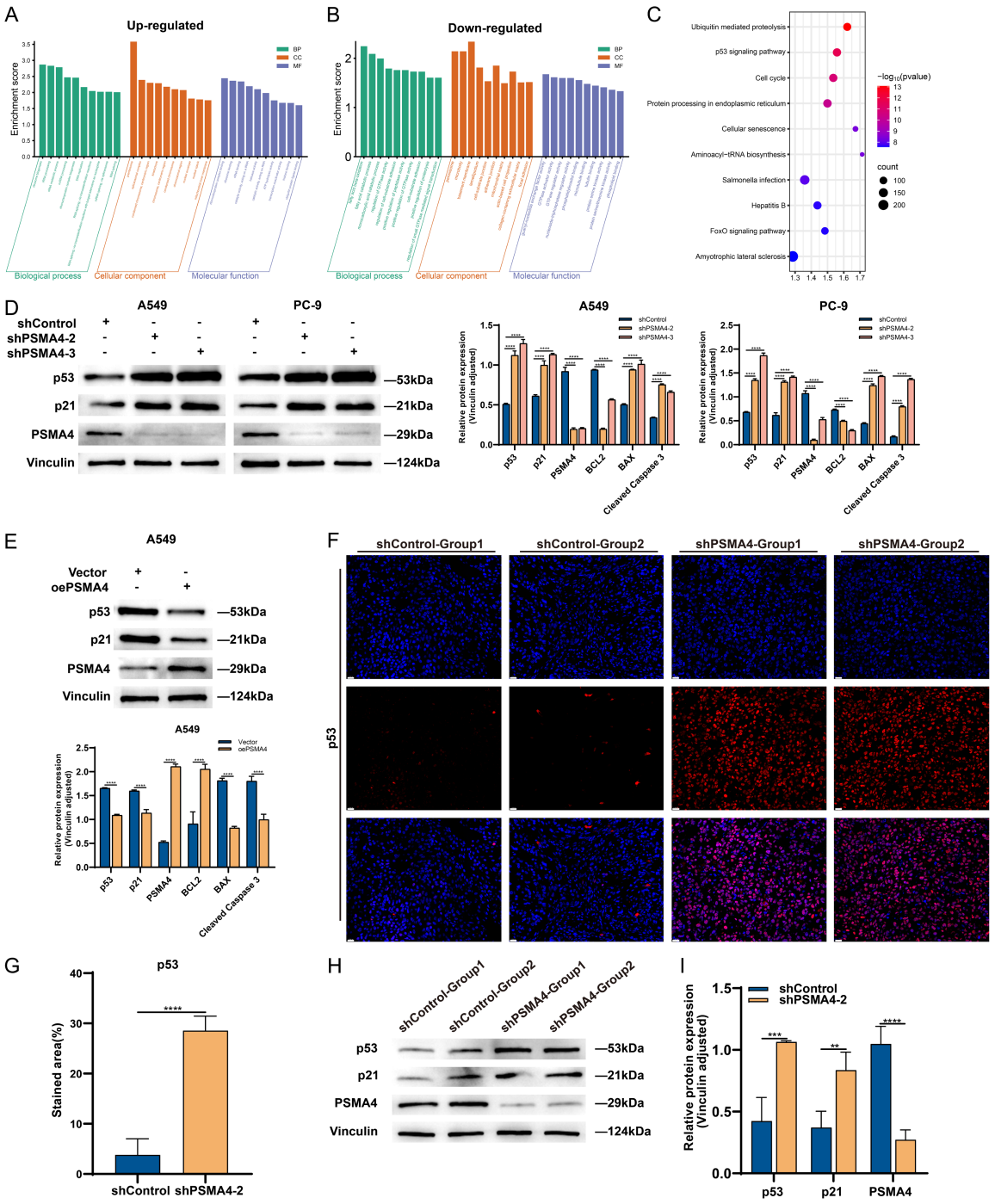

Figure 9. PSMA4 is associated with p53 signaling in LUAD cells and xenograft tumors. (A) The up-regulated pathways in GO enrichment analysis. (B) The down-regulated pathways in GO enrichment analysis. (C) KEGG enrichment analysis results. (D) Using A549 and PC-9 control and knockdown cells, the proteins were extracted and WB was used to detect the expression of p53 and p21 proteins. (E) Using control and overexpressed A549 cells, the proteins were extracted and WB was used to detect the expression of p53 and p21 proteins. (F, G) IF was used to detect the expression levels of p53 in the two groups of tumors. Original magnification, 400×, Scale bar = 20 μm. (H, I) WB was used to detect the expression of p53 and p21 proteins in the tumor tissues of the two groups of nude mice. Data is presented as the mean ± SD (***P* < 0.01, ****P* < 0.001, *****P* < 0.0001, D were analyzed using *One-way ANOVA*, while (E, G and I) were analyzed using unpaired Student's *t*-test). Abbreviations: LUAD, lung adenocarcinoma; GO, Gene Ontology; KEGG, Kyoto Encyclopedia of Genes and Genomes; IF, immunofluorescence; WB, Western blotting.

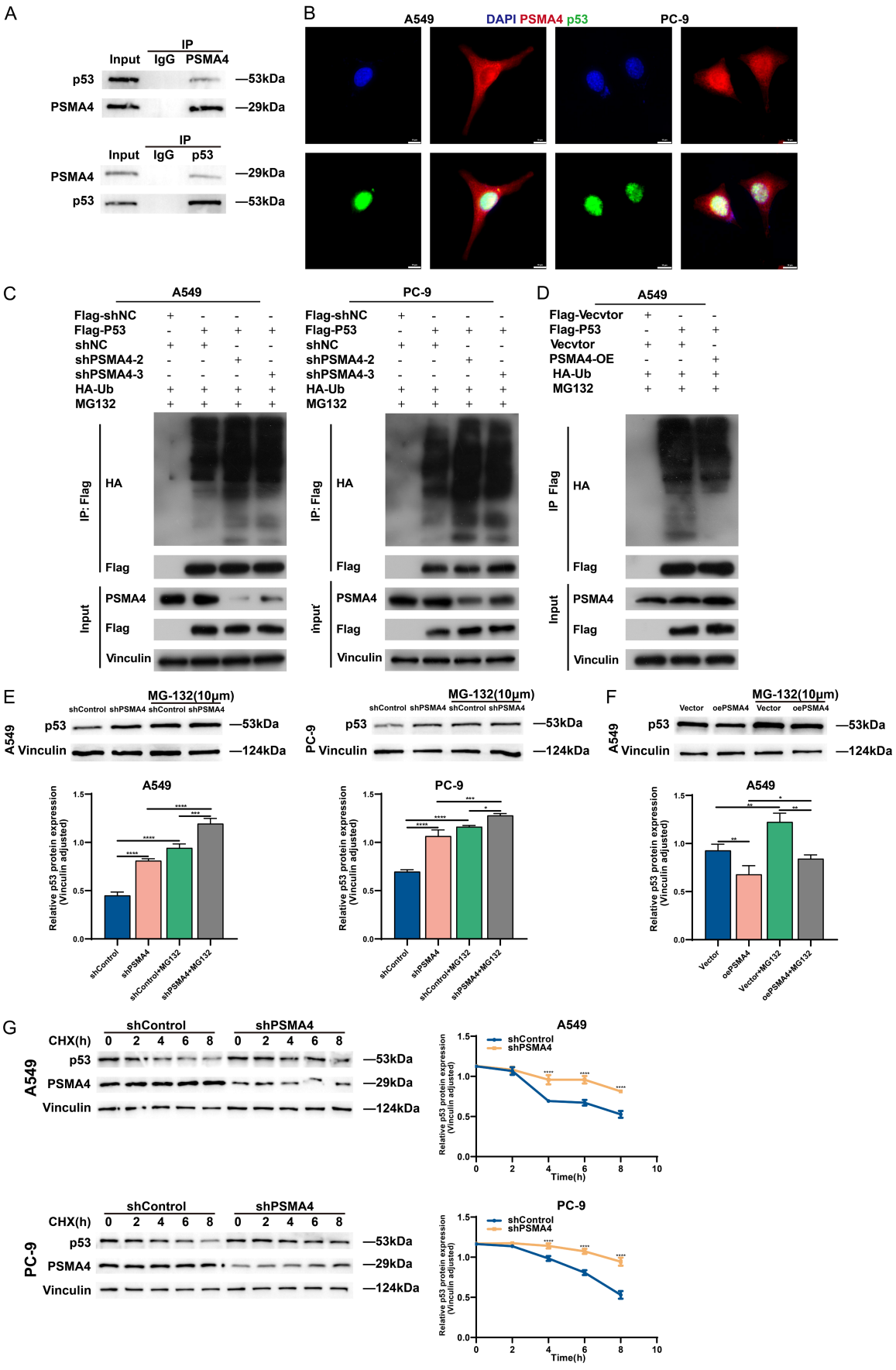
A
IP
Input IgG PSMA4
p53
PSMA4
—53kDa
—29kDa
IP
Input IgG p53
PSMA4
p53
—29kDa
—53kDa
B
A549
DAPI PSMA4 p53
PC-9
C
A549
Flag-shNC + - - -
Flag-P53 - + + +
shNC + + - -
shPSMA4-2 - - + -
shPSMA4-3 - - - +
HA-Ub + + + +
MG132 + + + +
IP: Flag
HA
Flag
Input
PSMA4
Flag
Vinculin
PC-9
Flag-shNC + - - -
Flag-P53 - + + +
shNC + + - -
shPSMA4-2 - - + -
shPSMA4-3 - - - +
HA-Ub + + + +
MG132 + + + +
IP: Flag
HA
Flag
Input
PSMA4
Flag
Vinculin
D
A549
Flag-Vecvtor + - -
Flag-P53 - + +
Vecvtor + + -
PSMA4-OE - - +
HA-Ub + + +
MG132 + + +
IP Flag
HA
Flag
Input
PSMA4
Flag
Vinculin
E
MG-132(10μm)
shControl shPSMA4 shControl shPSMA4
A549
p53
Vinculin
—53kDa
—124kDa
MG-132(10μm)
shControl shPSMA4 shControl shPSMA4
PC-9
p53
Vinculin
—53kDa
—124kDa
A549
Relative p53 protein expression (Vinculin adjusted)
shControl
shPSMA4
shControl+MG132
shPSMA4+MG132
PC-9
Relative p53 protein expression (Vinculin adjusted)
shControl
shPSMA4
shControl+MG132
shPSMA4+MG132
F
MG-132(10μm)
Vector oePSMA4 Vector oePSMA4
A549
p53
Vinculin
—53kDa
—124kDa
A549
Relative p53 protein expression (Vinculin adjusted)
Vector
oePSMA4
Vector+MG132
oePSMA4+MG132
G
shControl
shPSMA4
CHX(h) 0 2 4 6 8 0 2 4 6 8
A549
p53
PSMA4
Vinculin
—53kDa
—29kDa
—124kDa
A549
shControl
shPSMA4
Relative p53 protein expression (Vinculin adjusted)
Time(h)
shControl
shPSMA4
CHX(h) 0 2 4 6 8 0 2 4 6 8
PC-9
p53
PSMA4
Vinculin
—53kDa
—29kDa
—124kDa
PC-9
shControl
shPSMA4
Relative p53 protein expression (Vinculin adjusted)
Time(h)

Figure 10. PSMA4 interacts with p53 and facilitates the proteasome-dependent turnover of ubiquitinated p53. (A) Co-IP analysis showing the interaction between PSMA4 and p53. (B) IF staining showing the nuclear co-localization of PSMA4 and p53. Original magnification, 1000×, Scale bar = 10 μm. (C, D) Ubiquitination assays showing that PSMA4 knockdown increases, whereas PSMA4 overexpression decreases, the abundance of ubiquitinated p53. (E) WB analysis showing that p53 accumulation in PSMA4-knockdown A549 and PC-9 cells is further enhanced by MG132 treatment. (F) WB analysis showing that MG132 restores p53 accumulation in PSMA4-overexpressing A549 cells. (G) CHX chase assay showing that PSMA4 knockdown delays p53 degradation. Data is presented as the mean ± SD (***P* < 0.01, ****P* < 0.001, *****P* < 0.0001, (E and F) were analyzed using *One-way ANOVA*, while (G) were analyzed using repeated measures ANOVA). Abbreviations: LUAD, lung adenocarcinoma; Co-IP, Co-immunoprecipitation; IF, immunofluorescence; WB, Western blotting; MG132, proteasome inhibitor; CHX, Cycloheximide.

our multi-layer prioritization framework integrating genetic, transcriptomic, and clinical evidence, PSMA4 was selected as the leading candidate for functional validation.

Integrative trajectory and colocalization analyses indicated that an elevated PSMA4 expression level is associated with an increased risk of lung cancer development. Conversely, genetic variants in the PSMA4 promoter possibly mediate DNAm, downregulating its expression and correspondingly attenuating LUAD risk. Additional studies using public online databases consistently confirmed elevated PSMA4 expression in lung cancer tissues, which further supported its role as a candidate oncogene.

PSMA4 forms part of a highly ordered ring-shaped complex comprising 28 nonidentical subunits arranged into four stacked rings, and it is located on the chromosome 15q25.1 locus. Previous studies have confirmed that PSMA4 participates in various pathological processes. By using MR, Chen et al. found that an elevated PSMA4 expression level is correlated with abdominal aortic aneurysm risk, with colocalization supporting a shared genetic basis for the role of PSMA4 in both abdominal and intracranial aneurysms [35]. In immune and inflammatory contexts, Zhao et al. conducted transcriptomic analysis of Affymetrix data and identified PSMA4 - along with PSMA6 - as a potential modulator of ankylosing spondylitis progression [36]. Similarly, based on GWAS analysis, Sakornsakolpat et al. linked PSMA expression in blood and lung tissue to severe COPD [37], whereas Xia et al. used MR to correlate increased PSMA4 expression with sepsis susceptibility, suggesting a causal role and potential of PSMA4 as a therapeutic target [38]. In oncology, PSMA4 is associated with tumor immune escape. Phosphorylation of serine at position 188 of PSMA4 leads to the degradation of cGAS (a key cytosolic DNA sensor in innate immunity), which helps tumor growth by inhibiting interferon production and anti-tumor immunity [39]. Early GWAS by Amos et al. O'Brien et al. identified 15q25.1 and PSMA4 as lung cancer risk loci [40, 41]. Recently, Luan et al. used blood expression quantitative trait locus data in Mendelian randomization and proposed that PSMA4 is a promising therapeutic target for lung cancer [42], which is consistent with our study. After SMR and colocalization analysis, our study found that there is an association between PSMA4 at 15q25 and lung cancer risk, which goes beyond the previous locus associations, providing mechanistic insights and genetic value for its role in lung cancer development. To verify the association between PSMA4 and LUAD, IHC was performed on clinical samples, confirming that partial overexpression of PSMA4 in tumors compared with paired normal tissues. Subsequently, PSMA4 knockdown and overexpression models were constructed in LUAD cells. Functional experiments such as cell counting kit-8 (CCK-8), EdU, colony formation, wound healing, and Transwell showed that PSMA4 expression enhances the proliferation, migration, and invasion of LUAD cells in vitro. Xenograft experiments in vivo support these findings, and PSMA4 knockdown significantly inhibits tumor growth. IF detection of xenograft tissues shows that the expression of Ki-67 and vimentin is decreased in the knockdown group, and the expression of E-cadherin is increased, confirming that PSMA4 has a phenotype of promoting proliferation and invasion in vivo and is of great significance for the progression of LUAD.

PSMA4 encodes the proteasome core subunit and plays a core role in regulating inflammation, signal transduction and cell stress response [43]. As the main part of intracellular protein degradation, the proteasome controls multiple important processes, such as transcription, cell cycle progression and apoptosis

[44, 45]. The ubiquitin-proteasome system (UPS) can selectively regulate p53, regulate cell cycle arrest and apoptosis, and finally affect tumor progression [46]. Orlowski et al. pointed out that proteasome inhibitors can inhibit pro-apoptotic proteins such as p53 and Bax, and also reduce anti-apoptotic proteins such as Bcl-2, which then induces apoptosis in tumor cells [47]. In clinical practice, proteasome inhibitors such as. Bortezomib has obvious curative effects in hematological malignancies such as multiple myeloma. It also has anti-tumor activity in advanced solid tumors such as breast cancer, ovarian cancer, and prostate cancer, demonstrating the relevance of proteasomes in tumor treatment [48].

Our analysis of protein interactions also revealed a strong correlation between PSMA4 and TP53. Transcriptome sequencing results further demonstrated that PSMA4 is highly significantly and negatively correlated with the p53 signaling pathway. WB assay confirmed that PSMA4 modulates the expression of p53 pathway-related proteins. The p53 protein is a critical tumor suppressor and inhibits carcinogenesis by regulating cell cycle, apoptosis, metabolism, and DNA repair [49]. The *p53* gene is highly prone to mutation in cancer. The mutated *p53* gene is detected in approximately 50% of NSCLC cases and in more than 80% of small cell lung cancer cases [50]. Mutant p53 accelerates LUAD progression, whereas restoration of wild-type p53 suppresses advanced tumor growth [51]. p53 stability is precisely regulated by the UPS [52]. Under normal conditions, p53 is ubiquitinated through its negative regulator, the E3 ubiquitin ligase MDM2, and is degraded by the 26S proteasome [53, 54]. However, in certain tumors, UPS dysfunction induces excessive proteasome activation, leading to the overdegradation of tumor suppressor proteins such as p53 [55]. The UPS is involved in degrading most proteins in mammalian cells, with more than 19% of mutated oncogenic driver genes implicated in this process [56, 57]. Our Co-IP and immunofluorescence results demonstrated that PSMA4 interacts with p53 and co-localizes with it in the nucleus. In addition, PSMA4 knockdown increased the abundance of ubiquitinated p53, whereas PSMA4 overexpression reduced it. Importantly, MG132 treatment restored p53 accumulation, and CHX chase assays showed that the knockdown of PSMA4 would delay the degradation of p53. Collectively, these data support a model in which PSMA4 facilitates the proteasome-dependent turnover of ubiquitinated p53, thereby restraining p53 signaling.

Notably, our data do not demonstrate that PSMA4 directly catalyzes p53 ubiquitination or specifically targets a p53-E3 ligase complex for degradation. Rather, PSMA4 more likely contributes to the downstream degradation step after p53 has been ubiquitinated by upstream E3 ligases such as MDM2. This interpretation is more consistent with the established biology of the p53-MDM2-proteasome axis. It should also be noted that p53 degradation can occur through both ubiquitin-dependent and, in some contexts, ubiquitin-independent proteasomal mechanisms. Nevertheless, the combination of increased ubiquitinated p53 after PSMA4 knockdown, restoration of p53 accumulation by MG132, and delayed p53 turnover in CHX chase assays strongly supports a proteasome-dependent mechanism in our model. Future studies are warranted to determine whether PSMA4 affects the recruitment or processing of ubiquitinated p53 within the proteasome complex and whether canonical p53 regulators such as MDM2 are required for this effect.

In this study, we integrated SMR, colocalization analysis, bulk RNA-seq validation, and in vitro/in vivo experiments to prioritize and characterize PSMA4 as a LUAD-relevant candidate gene. To improve the robustness of our findings, we combined HEIDI testing, Bayesian colocalization, cross-cohort transcriptomic validation, and complementary analyses using multiple public databases. By leveraging large-scale GWAS datasets together with blood- and lung-derived QTL resources, our study provided broad data coverage and enhanced statistical power for gene prioritization. Importantly, the computational evidence was further supported by clinical IHC analysis, functional assays, xenograft experiments, and mechanistic studies demonstrating that PSMA4 facilitates the proteasome-dependent turnover of ubiquitinated p53. Although PPI analysis suggested potential associations between PSMA4 and other oncogenic drivers such as EGFR and KRAS, these interactions were not supported by consistent multi-omics or functional evidence in

our dataset. Future studies incorporating mutation-stratified models are needed to further investigate these potential regulatory relationships. Collectively, these results provide convergent genetic, transcriptomic, functional, and mechanistic evidence supporting PSMA4 as a biologically relevant and potentially actionable target in LUAD.

However, this study also has several limitations. Firstly, both SMR and colocalisation analyses rely on aggregated statistical data, and their inferential validity depends heavily on the quality and statistical power of the underlying GWAS and QTL data. If the original studies exhibit sample overlap, population structure bias or insufficient statistical power, this may introduce estimation bias. Furthermore, as the genetic data included in this study primarily originate from European populations, the generalisability of these findings to other ancestry groups requires validation through more diverse cohorts. Secondly, while our HEIDI test and colocalisation analysis aimed to minimise the risk of false associations due to LD or horizontal pleiotropy, it is not possible to entirely rule out the presence of multiple independent causal variants within LD regions or confounding associations through unmodelled pleiotropic pathways. Furthermore, colocalisation results are influenced by prior settings, LD references and systematic differences across data sources, meaning that low PP.H4 values do not entirely rule out genuine colocalisation relationships. Thirdly, due to limitations in current public data resources (e.g. the absence of eQTL data in the SMR Portal), the regional visualisation of certain genetic signals was incomplete. Furthermore, this study primarily focused on cis-regulatory variants, potentially overlooking biologically meaningful trans-regulatory signals. Finally, although functional experiments support PSMA4's role in promoting lung cancer progression, the specific upstream mechanisms by which it regulates the p53 pathway require further investigation. Although changes in E-cadherin and vimentin expression suggest a potential role of PSMA4 in Epithelial-mesenchymal transition (EMT), additional EMT-related markers (such as N-cadherin, Snail, and Slug) were not evaluated in this study. While PSMA4 was shown to regulate p53 and p21 expression, direct analysis of cell cycle distribution was not performed. Future studies are needed to determine the specific phases of the cell cycle affected by PSMA4. Although overexpression experiments were mainly performed in A549 cells, consistent knockdown effects observed in both A549 and PC-9 cells support the general role of PSMA4 in LUAD. Future studies should further validate these findings in additional cell lines. In summary, we propose that PSMA4 should be regarded as a candidate therapeutic target, supported by genetic and functional experimental evidence. Future studies should investigate the effects of PSMA4 inhibition, including pharmacological approaches and synergistic interactions with existing treatments such as EGFR-TKIs. Given that proteasome inhibitors (e.g., bortezomib) have demonstrated anti-tumor effects, targeting specific proteasome subunits such as PSMA4 may represent a more selective therapeutic strategy. Its definitive therapeutic value and clinical translation pathways require further exploration in subsequent studies.

Conclusions

Leveraging SMR analysis, multi-omics validation, and functional experiments, this study prioritizes PSMA4 as a genetically supported candidate target in lung adenocarcinoma. Integrated transcriptomic, in vitro, in vivo, and mechanistic analyses indicate that PSMA4 exerts oncogenic effects by promoting proliferation, migration, and invasion of LUAD cells. Importantly, our findings further suggest that PSMA4 interacts with p53 and facilitates the proteasome-dependent turnover of ubiquitinated p53, thereby suppressing p53 signaling. Together, these results support PSMA4 as a candidate therapeutic target and provide a mechanistic rationale for further translational investigation in LUAD.

Acknowledgements

We sincerely thank the authors of the publicly available datasets used in this research and also thank the First Affiliated Hospital of Anhui Medical University for providing us with the research platform. We also express our gratitude to the patients and their families who participated in this research for their support and cooperation in the study. We also extend our respect to the participants and researchers of this study. We would like to thank TopEdit (www.topeditsci.com) for its linguistic assistance dur-

ing the preparation of this manuscript. This study was supported by Clinical Medical Research and Transformation Special Project of the Science and Technology Department of Anhui Province (No. 202304295107020047) and Research Fund of Anhui Provincial Translational Medicine Research Institute (No. 2023zhyxC52).

Written informed consent was obtained from all patients prior to tissue collection.

Disclosure of conflict of interest

None.

Abbreviations

LUAD, lung adenocarcinoma; NSCLC, non-small cell lung cancer; SMR, Summary-Data-Based Mendelian Randomization; GWAS, genome-wide association studies; eQTL, expression quantitative trait loci; mQTL, methylation quantitative trait loci; HEIDI, Heterogeneity in Dependent Instruments; GEO, Gene Expression Omnibus; PPI, protein-protein interaction; PFS, progression-free survival; OS, overall survival; SNPs, single nucleotide polymorphisms; IVs, instrumental variables; LDL-C, low-density lipoprotein cholesterol; KD, knockdown; OE, overexpression; qPCR, Quantitative Real-time PCR; SPF, specific pathogen-free; GO, Gene Ontology; KEGG, Kyoto Encyclopedia of Genes and Genomes; IHC, immunohistochemistry; IF, immunofluorescence; DNAm, DNA methylation; GTEx, Genotype-Tissue Expression; FDR, false discovery rate; LD, linkage disequilibrium; GEPIA, Gene Expression Profiling Interactive Analysis; COPD, chronic obstructive pulmonary disease; PSMA4, Proteasome 20S Subunit Alpha 4; IREB2, Iron Responsive Element Binding Protein 2; UPS, ubiquitin-proteasome system; EMT, Epithelial-mesenchymal transition.

Address correspondence to: Drs. Renquan Zhang, Panpan Si and Ningning Kang, Department of Thoracic Surgery, The First Affiliated Hospital of Anhui Medical University, No. 218 Jixi Road, Hefei 230000, Anhui, China. E-mail: yfy113181@fy.ahmu.edu.cn (RQZ); yfy1131339@fy.ahmu.edu.cn (PPS); yfy1131073@fy.ahmu.edu.cn (NNK)

References

[1] Han B, Zheng R, Zeng H, Wang S, Sun K, Chen R, Li L, Wei W and He J. Cancer incidence and mortality in China, 2022. J Natl Cancer Cent 2024; 4: 47-53.

[2] Chen PX, Liu YH, Wen YK and Zhou CC. Non-small cell lung cancer in China. Cancer Commun (Lond) 2022; 42: 937-970.

[3] Herbst RS, Morgensztern D and Boshoff C. The biology and management of non-small cell lung cancer. Nature 2018; 553: 446-454.

[4] Chen WQ, Li H, Sun KX, Zheng RS, Zhang SW, Zeng HM, Zou XN, Gu XY and He J. Report of cancer incidence and mortality in China, 2014. Zhonghua Zhong Liu Za Zhi 2018; 40: 5-13.

[5] Ma L, Xue X, Zhang X, Yu K, Xu X, Tian X, Miao Y, Meng F, Liu X, Guo S, Qiu S, Wang Y, Cui J, Guo W, Li Y, Xia J, Yu Y and Wang J. The essential roles of m6A RNA modification to stimulate ENO1-dependent glycolysis and tumorigenesis in lung adenocarcinoma. J Exp Clin Cancer Res 2022; 41: 36.

[6] Nicholson AG, Tsao MS, Beasley MB, Borczuk AC, Brambilla E, Cooper WA, Dacic S, Jain D, Kerr KM, Lantuejoul S, Noguchi M, Papotti M, Rekhtman N, Scagliotti G, van Schil P, Sholl L, Yatabe Y, Yoshida A and Travis WD. The 2021 WHO classification of lung tumors: impact of advances since 2015. J Thorac Oncol 2022; 17: 362-387.

[7] Hirsch FR, Scagliotti GV, Mulshine JL, Kwon R, Curran WJ Jr, Wu YL and Paz-Ares L. Lung cancer: current therapies and new targeted treatments. Lancet 2016; 389: 299-311.

[8] Tsao AS, Scagliotti GV, Bunn PA Jr, Carbone DP, Warren GW, Bai C, de Koning HJ, Yousaf-Khan AU, McWilliams A, Tsao MS, Adusumilli PS, Rami-Porta R, Asamura H, Van Schil PE, Darling GE, Ramalingam SS, Gomez DR, Rosenzweig KE, Zimmermann S, Peters S, Ignatius Ou SH, Reungwetwattana T, Jänne PA, Mok TS, Wakelee HA, Pirker R, Mazières J, Brahmer JR, Zhou Y, Herbst RS, Papadimitrakopoulou VA, Redman MW, Wynes MW, Gandara DR, Kelly RJ, Hirsch FR and Pass HI. Scientific advances in lung cancer 2015. J Thorac Oncol 2016; 11: 613-638.

[9] Soria JC, Ohe Y, Vansteenkiste J, Reungwetwattana T, Chewaskulyong B, Lee KH, Dechaphunkul A, Imamura F, Nogami N, Kurata T, Okamoto I, Zhou C, Cho BC, Cheng Y, Cho EK, Voon PJ, Planchard D, Su WC, Gray JE, Lee SM, Hodge R, Marotti M, Rukazenkov Y and Ramalingam SS; FLAURA Investigators. Osimertinib in untreated EGFR-mutated advanced non-small-cell lung cancer. N Engl J Med 2018; 378: 113-125.

[10] Borghaei H, Paz-Ares L, Horn L, Spigel DR, Steins M, Ready NE, Chow LQ, Vokes EE, Felip E, Holgado E, Barlesi F, Kohlhäufl M, Arrieta O, Burgio MA, Fayette J, Lena H, Poddubskaya E, Gerber DE, Gettinger SN, Rudin CM, Rizvi N,

Crinò L, Blumenschein GR Jr, Antonia SJ, Dorange C, Harbison CT, Graf Finckenstein F and Brahmer JR. Nivolumab versus docetaxel in advanced nonsquamous non-small-cell lung cancer. N Engl J Med 2015; 373: 1627-39.

[11] Reck M, Rodríguez-Abreu D, Robinson AG, Hui R, Csőszi T, Fülöp A, Gottfried M, Peled N, Tafreshi A, Cuffe S, O'Brien M, Rao S, Hotta K, Leiby MA, Lubiniecki GM, Shentu Y, Rangwala R and Brahmer JR; KEYNOTE-024 Investigators. Pembrolizumab versus chemotherapy for PD-L1-positive non-small-cell lung cancer. N Engl J Med 2016; 375: 1823-1833.

[12] Zaretsky JM, Garcia-Diaz A, Shin DS, Escuin-Ordinas H, Hugo W, Hu-Lieskovan S, Torrejon DY, Abril-Rodriguez G, Sandoval S, Barthly L, Saco J, Homet Moreno B, Mezzadra R, Chmielowski B, Ruchalski K, Shintaku IP, Sanchez PJ, Puig-Saus C, Cherry G, Seja E, Kong X, Pang J, Berent-Maoz B, Comin-Anduix B, Graeber TG, Tumeh PC, Schumacher TN, Lo RS and Ribas A. Mutations associated with acquired resistance to PD-1 blockade in melanoma. N Engl J Med 2016; 375: 819-29.

[13] Hellmann MD, Paz-Ares L, Bernabe Caro R, Zurawski B, Kim SW, Carcereny Costa E, Park K, Alexandru A, Lupinacci L, de la Mora Jimenez E, Sakai H, Albert I, Vergnenegre A, Peters S, Syrigos K, Barlesi F, Reck M, Borghaei H, Brahmer JR, O'Byrne KJ, Geese WJ, Bhagavatheeswaran P, Rabindran SK, Kasinathan RS, Nathan FE and Ramalingam SS. Nivolumab plus ipilimumab in advanced non-small-cell lung cancer. N Engl J Med 2019; 381: 2020-2031.

[14] Skoulidis F, Goldberg ME, Greenawalt DM, Hellmann MD, Awad MM, Gainor JF, Schrock AB, Hartmaier RJ, Trabucco SE, Gay L, Ali SM, Elvin JA, Singal G, Ross JS, Fabrizio D, Szabo PM, Chang H, Sasson A, Srinivasan S, Kirov S, Szustakowski J, Vitazka P, Edwards R, Bufill JA, Sharma N, Ou SI, Peled N, Spigel DR, Rizvi H, Aguilar EJ, Carter BW, Erasmus J, Halpenny DF, Plodkowski AJ, Long NM, Nishino M, Denning WL, Galan-Cobo A, Hamdi H, Hirz T, Tong P, Wang J, Rodriguez-Canales J, Villalobos PA, Parra ER, Kalhor N, Sholl LM, Sauter JL, Jungbluth AA, Mino-Kenudson M, Azimi R, Elamin YY, Zhang J, Leonardi GC, Jiang F, Wong KK, Lee JJ, Papadimitrakopoulou VA, Wistuba II, Miller VA, Frampton GM, Wolchok JD, Shaw AT, Jänne PA, Stephens PJ, Rudin CM, Geese WJ, Albacker LA and Heymach JV. STK11/LKB1 mutations and PD-1 inhibitor resistance in KRAS-mutant lung adenocarcinoma. Cancer Discov 2018; 8: 822-835.

[15] Bowden J and Holmes MV. Meta-analysis and mendelian randomization: a review. Res Synth Methods 2019; 10: 486-496.

[16] Sekula P, Del Greco MF, Pattaro C and Köttgen A. Mendelian randomization as an approach to assess causality using observational data. J Am Soc Nephrol 2016; 27: 3253-3265.

[17] Burgess S, Davey Smith G, Davies NM, Dudbridge F, Gill D, Glymour MM, Hartwig FP, Kutalik Z, Holmes MV, Minelli C, Morrison JV, Pan W, Relton CL and Theodoratou E. Guidelines for performing Mendelian randomization investigations: update for summer 2023. Wellcome Open Res 2023; 4: 186.

[18] Wu Y, Zeng J, Zhang F, Zhu Z, Qi T, Zheng Z, Lloyd-Jones LR, Marioni RE, Martin NG, Montgomery GW, Deary IJ, Wray NR, Visscher PM, McRae AF and Yang J. Integrative analysis of omics summary data reveals putative mechanisms underlying complex traits. Nat Commun 2018; 9: 918.

[19] Zhu Z, Guo Y, Shi H, Liu CL, Panganiban RA, Chung W, O'Connor LJ, Himes BE, Gazal S, Hasegawa K, Camargo CA Jr, Qi L, Moffatt MF, Hu FB, Lu Q, Cookson WOC and Liang LM. Shared genetic and experimental links between obesity-related traits and asthma subtypes in UK Biobank. J Allergy Clin Immunol 2020; 145: 537-549.

[20] Yang Y, Dong L, Li Y, Huang Y and Zeng X. Summary data-based Mendelian randomization and single-cell RNA sequencing analyses identify immune associations with low-level LGALS9 in sepsis. J Cell Mol Med 2024; 28: e18559.

[21] Zheng J, Haberland V, Baird D, Walker V, Haycock PC, Hurle MR, Gutteridge A, Erola P, Liu Y, Luo S, Robinson J, Richardson TG, Staley JR, Elsworth B, Burgess S, Sun BB, Danesh J, Runz H, Maranville JC, Martin HM, Yarmolinsky J, Laurin C, Holmes MV, Liu JZ, Estrada K, Santos R, McCarthy L, Waterworth D, Nelson MR, Smith GD, Butterworth AS, Hemani G, Scott RA and Gaunt TR. Phenome-wide Mendelian randomization mapping the influence of the plasma proteome on complex diseases. Nat Genet 2020; 52: 1122-1131.

[22] Lin PW, Lin ZR, Wang WW, Guo AS and Chen YX. Identification of immune-inflammation targets for intracranial aneurysms: a multiomics and epigenome-wide study integrating summary-data-based Mendelian randomization, single-cell-type expression analysis, and DNA methylation regulation. Int J Surg 2025; 111: 346-359.

[23] Zhu Z, Zhang F, Hu H, Bakshi A, Robinson MR, Powell JE, Montgomery GW, Goddard ME, Wray NR, Visscher PM and Yang J. Integration of summary data from GWAS and eQTL studies predicts complex trait gene targets. Nat Genet 2016; 48: 481-487.

[24] Burgess S, Small DS and Thompson SG. A review of instrumental variable estimators for Mendelian randomization. Stat Methods Med Res 2017; 26: 2333-2355.
[25] Shin CJ, Wong S, Davis MJ and Ragan MA. Protein-protein interaction as a predictor of subcellular location. BMC Syst Biol 2009; 3: 28.
[26] Xia H, Wu Y, Zhao J, Cheng C, Lin J, Yang Y, Lu L, Xiang Q, Bian T and Liu Q. N6-Methyladenosine-modified circSAV1 triggers ferroptosis in COPD through recruiting YTHDF1 to facilitate the translation of IREB2. Cell Death Differ 2023; 30: 1293-1304.
[27] Khiroya H, Moore JS, Ahmad N, Kay J, Woolnough K, Langman G, Ismail I, Naidu B, Tselepis C and Turner AM. IRP2 as a potential modulator of cell proliferation, apoptosis and prognosis in nonsmall cell lung cancer. Eur Respir J 2017; 49: 1600711.
[28] Yamamoto K, Okamoto A, Isonishi S, Ochiai K and Ohtake Y. A novel gene, CRR9, which was up-regulated in CDDP-resistant ovarian tumor cell line, was associated with apoptosis. Biochem Biophys Res Commun 2001; 280: 1148-1154.
[29] McKay JD, Hung RJ, Gaborieau V, Boffetta P, Chabrier A, Byrnes G, Zaridze D, Mukeria A, Szeszenia-Dabrowska N, Lissowska J, Rudnai P, Fabianova E, Mates D, Bencko V, Foretova L, Janout V, McLaughlin J, Shepherd F, Montpetit A, Narod S, Krokan HE, Skorpen F, Elvestad MB, Vatten L, Njolstad I, Axelsson T, Chen C, Goodman G, Barnett M, Loomis MM, Lubiński J, Matyjasik J, Lener M, Oszutowska D, Field J, Liloglou T, Xinarianos G and Cassidy A; EPIC Study; Vineis P, Clavel-Chapelon F, Palli D, Tumino R, Krogh V, Panico S, González CA, Ramón Quirós J, Martínez C, Navarro C, Ardanaz E, Larrañaga N, Kham KT, Key T, Bueno-de-Mesquita HB, Peeters PH, Trichopoulou A, Linseisen J, Boeing H, Hallmans G, Overvad K, Tjønneland A, Kumle M, Riboli E, Zelenika D, Boland A, Delepine M, Foglio M, Lechner D, Matsuda F, Blanche H, Gut I, Heath S, Lathrop M, Brennan P. Lung cancer susceptibility locus at 5p15.33. Nat Genet 2008; 40: 1404-1406.
[30] Wang Y, Broderick P, Webb E, Wu X, Vijayakrishnan J, Matakidou A, Qureshi M, Dong Q, Gu X, Chen WV, Spitz MR, Eisen T, Amos CI and Houlston RS. Common 5p15.33 and 6p21.33 variants influence lung cancer risk. Nat Genet 2008; 40: 1407-1409.
[31] James MA, Vikis HG, Tate E, Rymaszewski AL and You M. CRR9/CLPTM1L regulates cell survival signaling and is required for ras transformation and lung tumorigenesis. Cancer Res 2014; 74: 1116-1127.
[32] Liu X, Song J, Zhang H, Liu X, Zuo F, Zhao Y, Zhao Y, Yin X, Guo X, Wu X, Zhang H, Xu J, Hu J, Jing J, Ma X and Shi H. Immune checkpoint HLA-E:CD94-NKG2A mediates evasion of circulating tumor cells from NK cell surveillance. Cancer Cell 2023; 41: 272-287, e9.
[33] Talebian Yazdi M, van Riet S, van Schadewijk A, Fiocco M, van Hall T, Taube C, Hiemstra PS and van der Burg SH. The positive prognostic effect of stromal CD8+ tumor-infiltrating T cells is restrained by the expression of HLA-E in non-small cell lung carcinoma. Oncotarget 2016; 7: 3477-88.
[34] Kim J, Hu Z, Cai L, Li K, Choi E, Faubert B, Bezwada D, Rodriguez-Canales J, Villalobos P, Lin YF, Ni M, Huffman KE, Girard L, Byers LA, Unsal-Kacmaz K, Peña CG, Heymach JV, Wauters E, Vansteenkiste J, Castrillon DH, Chen BPC, Wistuba I, Lambrechts D, Xu J, Minna JD and DeBerardinis RJ. CPS1 maintains pyrimidine pools and DNA synthesis in KRAS/LKB1-mutant lung cancer cells. Nature 2017; 546: 168-172.
[35] Chen Y, Xu X, Wang L, Li K, Sun Y, Xiao L, Dai J, Huang M, Wang Y and Wang DW. Genetic insights into therapeutic targets for aortic aneurysms: a Mendelian randomization study. EBioMedicine 2022; 83: 104199.
[36] Zhao H, Wang D, Fu D and Xue L. Predicting the potential ankylosing spondylitis-related genes utilizing bioinformatics approaches. Rheumatol Int 2015; 35: 973-979.
[37] Sakornsakolpat P, Morrow JD, Castaldi PJ, Hersh CP, Bossé Y, Silverman EK, Manichaikul A and Cho MH. Integrative genomics identifies new genes associated with severe COPD and emphysema. Respir Res 2018; 19: 46.
[38] Xia R, Sun M, Yin J, Zhang X and Li J. Using Mendelian randomization provides genetic insights into potential targets for sepsis treatment. Sci Rep 2024; 14: 8467.
[39] Rao K, Zhang X, Luo Y, Xia Q, Jin Y and He J. Lactylation orchestrates ubiquitin-independent degradation of cGAS and promotes tumor growth. Cell Rep 2025; 44: 115441.
[40] Amos CI, Gorlov IP, Dong Q, Wu X, Zhang H, Lu EY, Scheet P, Greisinger AJ, Mills GB and Spitz MR. Nicotinic Acetylcholine receptor region on chromosome 15q25 and lung cancer risk among African Americans: a case-control study. J Natl Cancer Inst 2010; 102: 1199-1205.
[41] O'Brien TD, Jia P, Caporaso NE, Landi MT and Zhao Z. Weak sharing of genetic association signals in three lung cancer subtypes: evidence at the SNP, gene, regulation, and pathway levels. Genome Med 2018; 10: 16.
[42] Luan Y, Xian D, Zhao C, Qing X, He H, Zheng K, Song W, Jiang T, Wang W and Duan C. Therapeutic targets for lung cancer: genome-wide Mendelian randomization and coloca-

lization analyses. Front Pharmacol 2024; 15: 1441233.
[43] Liu Y, Liu P, Wen W, James MA, Wang Y, Bailey-Wilson JE, Amos CI, Pinney SM, Yang P, de Andrade M, Petersen GM, Wiest JS, Fain PR, Schwartz AG, Gazdar A, Gaba C, Rothschild H, Mandal D, Kupert E, Lee J, Seminara D, Minna J, Anderson MW and You M. Haplotype and cell proliferation analyses of candidate lung cancer susceptibility genes on chromosome 15q24-25.1. Cancer Res 2009; 69: 7844-7850.
[44] Bard JAM, Goodall EA, Greene ER, Jonsson E, Dong KC and Martin A. Structure and function of the 26S proteasome. Annu Rev Biochem 2018; 87: 697-724.
[45] Stana F, Vujovic M, Mayaki D, Leduc-Gaudet JP, Leblanc P, Huck L and Hussain SNA. Differential regulation of the autophagy and proteasome pathways in skeletal muscles in sepsis. Crit Care Med 2017; 45: e971-e979.
[46] Bedford L, Lowe J, Dick LR, Mayer RJ and Brownell JE. Ubiquitin-like protein conjugation and the ubiquitin-proteasome system as drug targets. Nat Rev Drug Discov 2011; 10: 29-46.
[47] Orlowski RZ and Kuhn DJ. Proteasome inhibitors in cancer therapy: lessons from the first decade. Clin Cancer Res 2008; 14: 1649-1657.
[48] Yang H, Zonder JA and Dou QP. Clinical development of novel proteasome inhibitors for cancer treatment. Expert Opin Investig Drugs 2009; 18: 957-971.
[49] Aubrey BJ, Kelly GL, Janic A, Herold MJ and Strasser A. How does p53 induce apoptosis and how does this relate to p53-mediated tumour suppression? Cell Death Differ 2018; 25: 104-113.
[50] Cancer Genome Atlas Research Network. Comprehensive molecular profiling of lung adenocarcinoma. Nature 2014; 511: 543-550.
[51] Chen T, Ashwood L, Kondrashova O, Strasser A, Kelly G and Sutherland KD. Breathing new insights into the role of mutant p53 in lung cancer. Oncogene 2025; 44: 115-129.
[52] Gao Y, Chen B, Wang R, Xu A, Wu L, Lu H and Zhao G. Knockdown of RRM1 in tumor cells promotes radio-/chemotherapy induced ferroptosis by regulating p53 ubiquitination and p21-GPX4 signaling axis. Cell Death Discov 2022; 8: 343.
[53] Haupt Y, Maya R, Kazaz A and Oren M. Mdm2 promotes the rapid degradation of p53. Nature 1997; 387: 296-299.
[54] He Y, Huang J, Wang P, Shen X, Li S, Yang L, Liu W, Suksamrarn A, Zhang G and Wang F. Emodin potentiates the antiproliferative effect of interferon α/β by activation of JAK/STAT pathway signaling through inhibition of the 26S proteasome. Oncotarget 2016; 7: 4664-4679.
[55] Wu D, Miao J, Hu J, Li F, Gao D, Chen H, Feng Y, Shen Y and He A. PSMB7 Is a Key Gene Involved in the Development of multiple myeloma and resistance to bortezomib. Front Oncol 2021; 11: 684232.
[56] Collins GA and Goldberg AL. The logic of the 26S proteasome. Cell 2017; 169: 792-806.
[57] Tokheim C, Wang X, Timms RT, Zhang B, Mena EL, Wang B, Chen C, Ge J, Chu J, Zhang W, Elledge SJ, Brown M and Liu XS. Systematic characterization of mutations altering protein degradation in human cancers. Mol Cell 2021; 81: 1292-1308, e11.

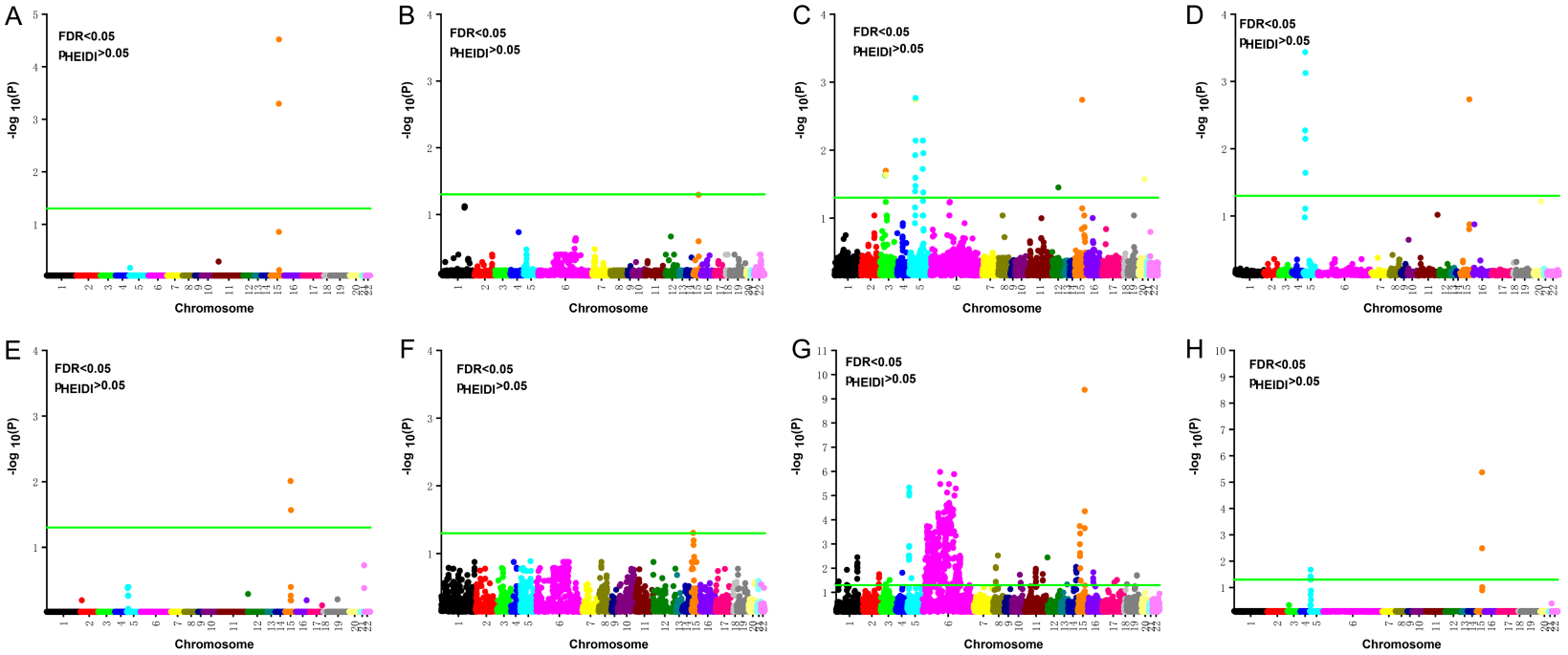

Figure S1. Manhattan plots of significant results from summary data-based Mendelian randomization in overall lung cancer. A-H represent the aggregated results of SMR calculations conducted separately by each GWAS dataset (finngen_R10:C3_NSCLC_ADENO_EXALLC, C3_NSCLC_SQUAM_EXALLC, C3_BRONCHUS_LUNG_EX-ALLC, C3_LUNG_NONSMALL_EXALLC, ukbb: LUNG_CANCER,ieu: ukb-b-20176, ukb-b-14521, ieu_b_4955) with mQTL datasets(McRae _Blood).The green solid line indicates *P*-value threshold after false discovery rate is 0.05, FDR < 0.05, p_HEIDI > 0.05. Abbreviations: SMR, summary data-based Mendelian randomization; GWAS, the genome-wide association study; mQTL, methylation Quantitative Trait Loci; FDR, false discovery rate; HEIDI test, heterogeneity in dependent instruments test.

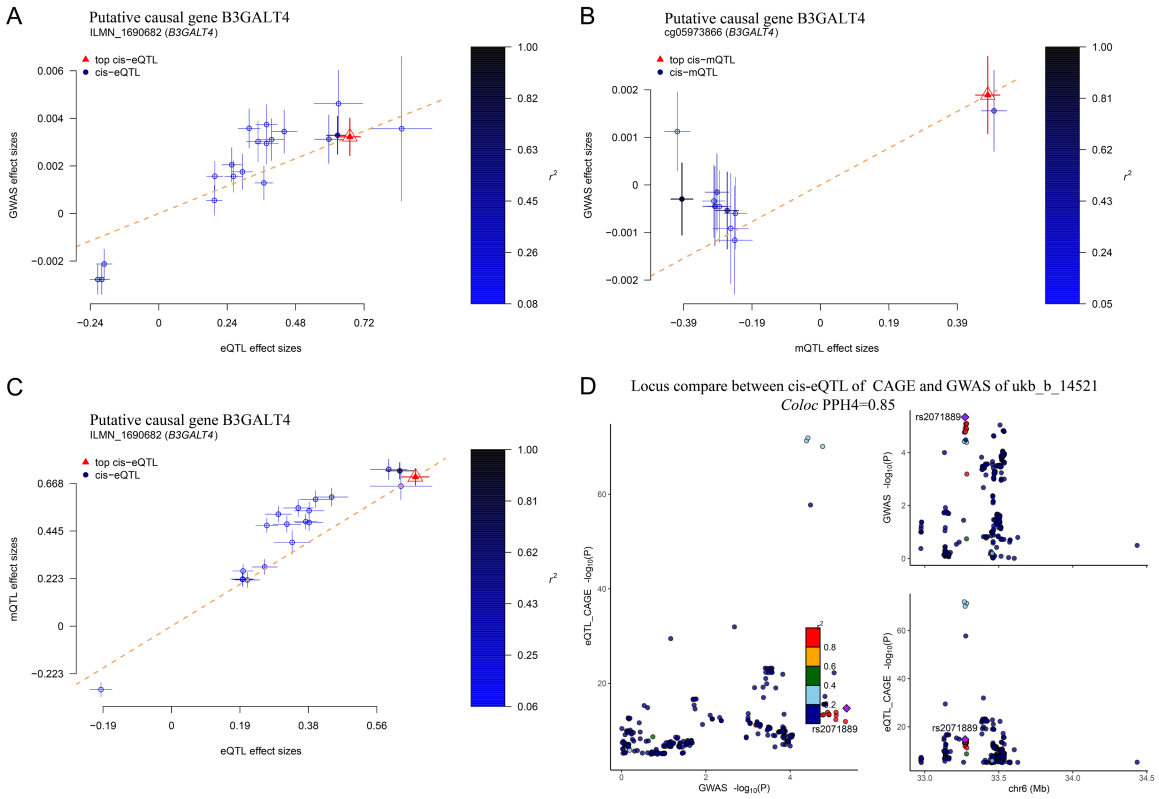

Figure S2. Based on the results of SMR, a correlation analysis and co-localization analysis were conducted between the GWAS datasets of ieu: ukb-b-14521 with the eQTL dataset of CAGE and the mQTL dataset of McRae corresponding to B3GALT4. A-D. The correlation diagrams of eQTL-GWAS, mQTL-GWAS, eQTL-mQTL, and colocalization analyses. Abbreviations: SMR, summary data-based Mendelian randomization; GWAS, the genome-wide association study; eQTL, expression quantitative trait loci; mQTL, methylation Quantitative Trait Loci.

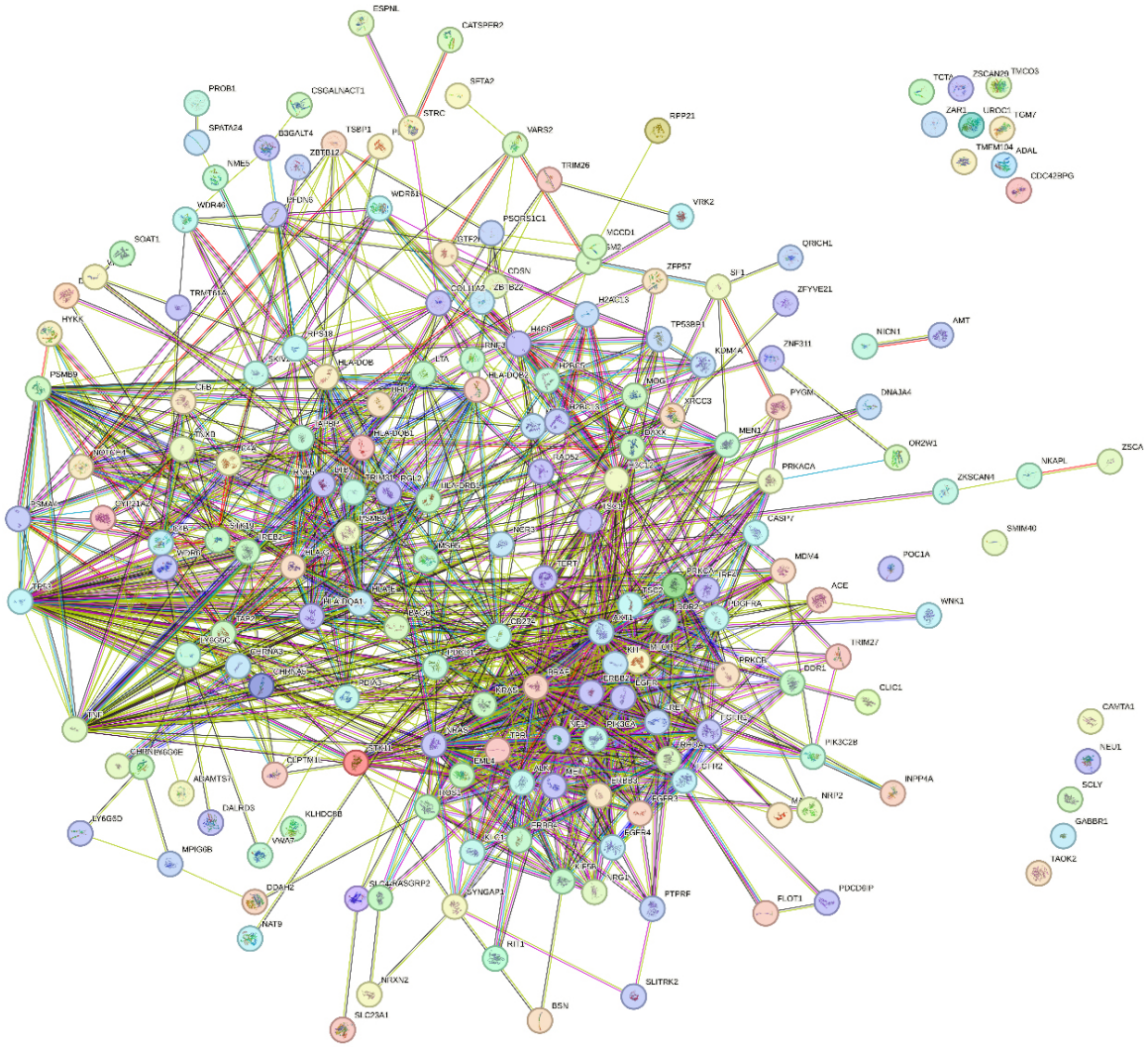

Figure S3. The PPI network of proteins identified by SMR. Lines represent interactions between proteins. Green line indicates gene neighborhood and predicted interaction; Blue line indicates known interaction from curated databases; Fuchsia line indicates known interaction that is experimentally determined. Black line indicates co-expression. Data information was from STRING database. Abbreviations: PPI, protein-protein interaction; SMR, summary data-based Mendelian randomization.

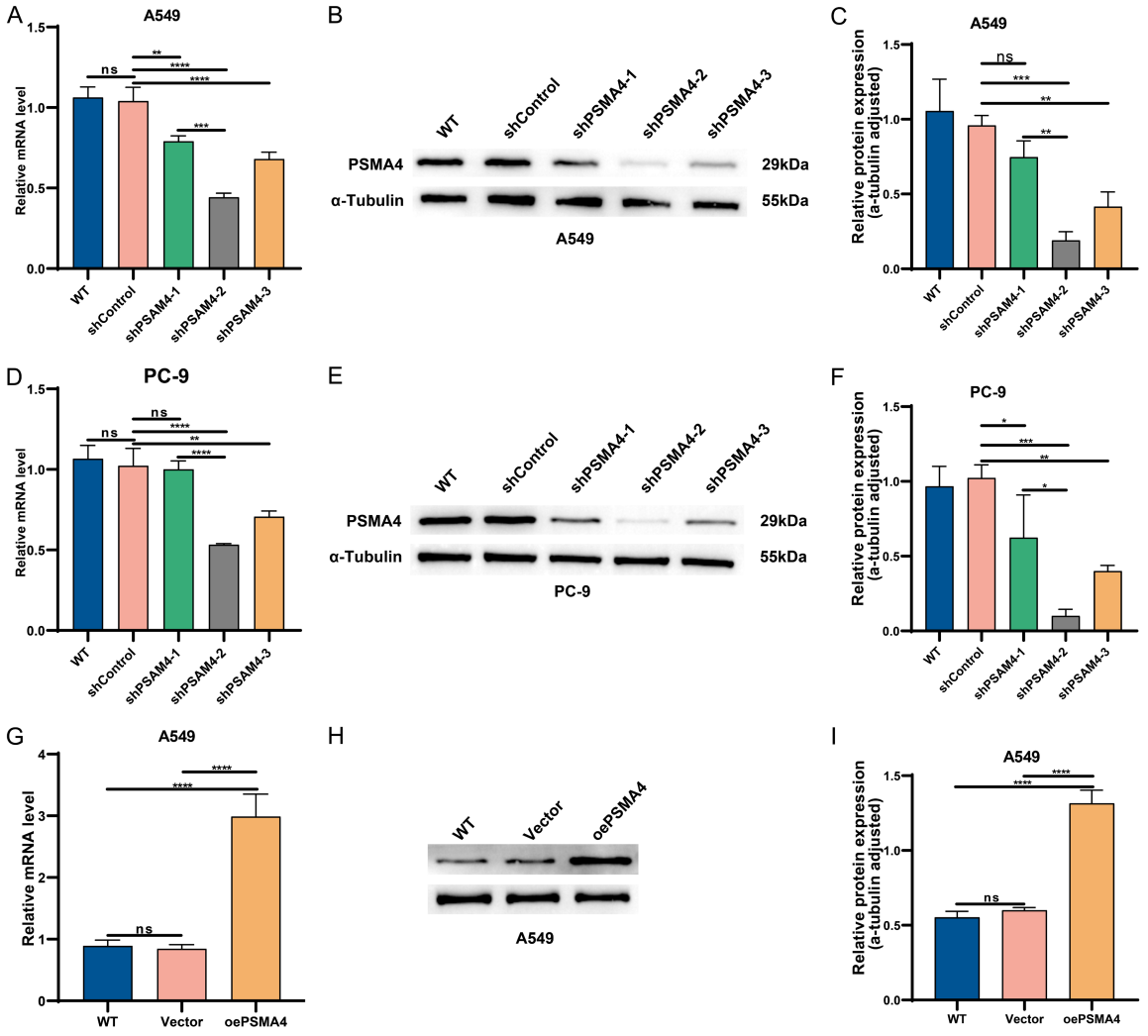

Figure S4. The efficiency of knockdown and overexpression of PSMA4 in LUAD cells. A. The qRT-PCR was used to detect the mRNA expression levels of PSMA4 in A549 cells with normal genotype (WT), control cells (shControl), and PSMA4 knockdown cells (sh PSMA4-1, sh PSMA4-2, and sh PSMA4-3). B, C. Western blot analysis of PSMA4 expression in A549 cells with normal genotype (WT), control cells (shControl), and PSMA4 knockdown cells (sh PSMA4-1, sh PSMA4-2, and sh PSMA4-3). D. qRT-PCR was used to detect the mRNA expression levels of PSMA4 in PC-9 cells with normal genotype (WT), control cells (shControl), and PSMA4 knockdown cells (sh PSMA4-1, sh PSMA4-2, and sh PSMA4-3). E, F. Western blot analysis of PSMA4 expression in A549 cells with normal genotype (WT), control cells (shControl), and PSMA4 knockdown cells (sh PSMA4-1, sh PSMA4-2, and sh PSMA4-3). G. qRT-PCR was used to detect the mRNA expression levels of PSMA4 in A549 cells with normal genotype (WT), control cells (Vector), and PSMA4 overexpression cells (oePSMA4). H, I. Western blot analysis of PSMA4 expression in A549 cells with normal genotype (WT), control cells (Vector), and PSMA4 overexpression cells (oePSMA4). Data is presented as the mean ± SD (***P* < 0.01, ****P* < 0.001, *****P* < 0.0001 by *One-way ANOVA*). Abbreviations: LUAD, lung adenocarcinoma; qRT-PCR, Quantitative Real-time PCR; WB, Western blotting.